The use of quasi-isospectral operators for damage detection in rods

Noname manuscript No.
(will be inserted by the editor)

The use of quasi-isospectral operators for damage detection in rods

Antonio Bilotta · Antonino Morassi · Emilio Turco

Received: date / Accepted: date

Abstract We consider the inverse problem of reconstructing the axial stiffness of a damaged rod from the knowledge of a finite number of resonant frequencies of the free axial vibration under supported end conditions. The damage is described as a reduction of the axial stiffness, and the undamaged and damaged configurations of the rod are assumed to be symmetric. The method is based on repeated determination of quasi-isospectral rod operators, that is rods which have the same spectrum of a given rod with the exception of a single resonant frequency which is free to move in a prescribed interval. The reconstruction procedure is explicit and it is numerically implemented and tested for the identification of single and multiple localized damages. The sensitivity of the technique to the number of frequencies used and to the shape, intensity and position of the damages, as well as to the presence of noise in the data, is evaluated and discussed. The effect of suitable filtering of the results based on a priori information on the physics of the problem is proposed. An experimental application to the identification of localized damage in a free-free steel rod is also presented.

A. Bilotta
Università della Calabria, Dipartimento di Ingegneria Informatica, Modellistica, Elettronica e Sistemistica (DIMES), via P. Bucci, 87036 Rende (CS), Italy.
E-mail: antonio.bilotta@unical.it

A. Morassi
Università di Udine, Dipartimento Politecnico di Ingegneria e Architettura, via Cotonificio 114, 33100 Udine (UD), Italy.
E-mail: antonino.morassi@uniud.it

E. Turco (corresponding author)
Università di Sassari, Dipartimento di Architettura, Design e Urbanistica (DADU), via Garibaldi 35, 07041 Alghero (SS), Italy.
E-mail: emilio.turco@uniss.it

Keywords Damage detection · Rods · Longitudinal vibrations · Quasi-isospectral operators · Analytical methods · Inverse problems

Mathematics Subject Classification (2000) 74 · 34 · 74H45 · 74G75 · 74K10 · 74S05

1 Introduction

Dynamic methods are a powerful tool for the identification of damage in structures [1,21,32,7]. By monitoring the dynamic response of a system in a referential (undamaged) and perturbed (damaged) state, one tries to detect the occurrence of possible changes in the system and determine the locations and intensities of the damage. In most of the practical applications, natural frequencies and principal mode shapes are used as input data. These dynamic parameters may be estimated either by classical experimental modal analysis or by operational modal analysis methods. If on the one hand the formulation of the diagnostic problem from dynamic data is relatively straightforward, on the other hand its solution still presents challenging issues and open questions, even in case of simple structural systems such as beams under axial or bending vibration [15]. The main source of difficulty is connected with the inverse nature of the diagnostic problem and, therefore, with the need of facing with the intrinsic ill-posedeness of the correspondent mathematical problem. Crucial questions are, among others, the uniqueness of the solution and the determination of efficient and robust reconstruction procedures. In addition, most of the general mathematical results available in the literature require an infinite amount of exact data for the identification of one-dimensional elements, whereas only a finite set of noisy-data is typically available in real-life applications.

Basing on the above considerations, it is fair to say that further efforts, both on the theoretical and applied side, are needed to reduce the gap between theory and application of vibrational-based damage identification methods. The present research is a contribution to this issue. We propose a method for the determination of damage in axially vibrating rods by using a finite number of natural frequencies belonging to a given set of end conditions. The method is of constructive type and it is based on the determination of suitable quasi-isospectral Sturm-Liouville operators. More precisely, let us consider an axially vibrating rod supported at both ends and having given axial stiffness $\widehat{p} = \widehat{p}(x)$ and mass density $\widehat{\rho} = \widehat{\rho}(x)$ in its undamaged state. A structural damage is modelled by a change (reduction) of the axial stiffness from $\widehat{p}$ to the unknown coefficient $p = p(x)$, without altering the mass density $\widehat{\rho}$. Under the assumption that both the undamaged and damaged systems are symmetric, that is $\widehat{p}$, p and $\widehat{\rho}$ are even functions with respect to the mid-point of the rod, we show how to construct the stiffness coefficient p such that the damaged rod $(p, \widehat{\rho})$ has exactly the prescribed (measured) values of the first N eigenfrequencies of the Dirichlet spectrum. Therefore, one expects to recover information about the damage from the behavior of the reconstructed coefficient p. It should be noticed that the analysis is restricted to symmetric rods since, in this case, the knowledge of the full Dirichlet spectrum determines uniquely the function p, provided that $\widehat{\rho}$ is given, see [19] and [24] for uniqueness results for more general type of second-order Sturm-Liouville operators.

Our reconstruction method differs from the techniques available in the mathematical literature on Sturm-Liouville inverse eigenvalue problems, see, for example, [16,4,27] and the book [15] for an update overview, and also from the variational/optimization-type methods usually employed to solve diagnostic problems from finite eigenfrequency data, see, among other contributions, [14,9,42,40,39,36,30,37,13,33]. The main idea of our approach is based on the explicit construction of quasi-isospectral rod operators which have exactly the same eigenvalues of a given rod with the exception of a single eigenvalue, which belongs to a prescribed interval. Starting from the undamaged rod, by keeping fixed all the eigenvalues apart from the nth, we find an axial stiffness coefficient in such a way this nth eigenvalue is shifted to the corresponding value assigned for the damaged rod. Then, using repeatedly the procedure, after a finite number of steps we will construct a rod with exactly the first N eigenfrequencies of the damaged rod. An analogous approach was exploited by us in [6] in the more simple context of Webster's horn equation $(Au')' + \lambda Au = 0$, in which only one coefficient - not two, as for the rod operator - is present.

The paper is organized as follows. The formulation of the diagnostic problem and the theoretical bases of the identification method are presented in Section 2 and 3, respectively. Section 4 contains the description of the reconstruction algorithm. Section 5 is devoted to the illustration of the results of a series of numerical simulations. The generalization to Neumann end conditions is discussed in Section 6, whereas Section 7 presents a possible post-filtering of the results based on additional a priori information about the physics of the problem. Section 8 contains an experimental validation of the proposed method on a free-free rod with a notch. For the sake of completeness, details on the construction of quasi-isospectral operators in impedance form are recalled in the Appendix.

2 Formulation of the problem

Let us consider a thin straight rod, having both the ends supported and unit length, in its undamaged state. The free, undamped, infinitesimal longitudinal vibrations are governed by the Sturm-Liouville $(\widehat{p}, \widehat{\rho})$-eigenvalue problem

$$(\widehat{p}v')' + \widehat{\lambda}\widehat{\rho}v = 0\,, \quad \text{in } (0,1)\,, \tag{1}$$

$$v(0) = 0 = v(1)\,, \tag{2}$$

where $v = v(x)$ is the amplitude and $\sqrt{\widehat{\lambda}}$ is the radian frequency of the vibration. Let the axial stiffness $\widehat{p} = \widehat{p}(x)$ and the mass density $\widehat{\rho} = \widehat{\rho}(x)$ satisfy the following assumptions:

$$\widehat{p} \in C^2([0,1]), \quad \widehat{p}(x) \geq \widehat{\alpha}_0 > 0 \quad \text{in } [0,1], \tag{3}$$

$$\widehat{\rho} \in C^2([0,1]), \quad \widehat{\rho}(x) \geq \widehat{\beta}_0 > 0 \quad \text{in } [0,1], \tag{4}$$

where $\widehat{\alpha}_0$, $\widehat{\beta}_0$ are given constants. Here, $C^k([0,1])$ is the space of continuous functions with continuous derivatives up to the order k, $k \geq 1$. We consider rods which are symmetrical with respect to the mid-point $x = \frac{1}{2}$, namely

$$\widehat{p}(x) = \widehat{p}(1-x), \quad \widehat{\rho}(x) = \widehat{\rho}(1-x) \quad \text{in } [0,1]. \tag{5}$$

Under the above assumptions, the Dirichlet eigenvalue problem (1)–(2) has a countable infinite sequence of eigenvalues $\{\widehat{\lambda}_m\}_{m=1}^{\infty}$, with $0 < \widehat{\lambda}_1 < \widehat{\lambda}_2 < \ldots$ and $\lim_{m\to\infty} \widehat{\lambda}_m = \infty$. Let us denote by $\widehat{v}_m(x)$ the eigenfunction associated to the mth eigenvalue.

Let us introduce the damaged configuration of the rod. It is assumed that the structural damage could be described as a variation (reduction) of the effective axial stiffness of the rod, without altering the mass density.

This assumption is rather common in damage detection studies and, in fact, a careful description of damage would be hardly worth doing since it would require a detailed knowledge of degradation, which is not always available in advance in inverse analysis. Therefore, the $(p,\widehat{\rho})$-eigenvalue problem for the damaged rod is assumed of the form

$$(pv')' + \lambda\widehat{\rho}v = 0, \quad \text{in } (0,1)\,, \tag{6}$$

$$v(0) = 0 = v(1)\,, \tag{7}$$

where the axial stiffness $p = p(x)$ satisfies the same regularity and positivity conditions of $\widehat{p}(x)$. Moreover, we restrict the analysis to symmetrical damaged rods, that is

$$p(x) = p(1-x) \quad \text{in } [0,1]. \tag{8}$$

As before, problem (6)–(7) admits an infinite sequence of positive and simple eigenvalues $\{\lambda_m\}_{m=1}^{\infty}$ with accumulation point at infinity and such that

$$\widehat{\lambda}_{m-1} \le \lambda_m \le \widehat{\lambda}_m\,, \tag{9}$$

for every $m \ge 1$, with $\widehat{\lambda}_0 = 0$.

Our diagnostic problem can be formulated as an inverse problem in vibration with finite eigenfrequency data: given the undamaged configuration of the rod (*e.g.*, $\widehat{p}(x)$ and $\widehat{\rho}(x)$ are given functions in $[0,1]$), we wish to determine the axial stiffness coefficient $p = p(x)$ from the knowledge of the first N eigenvalues $\{\lambda_m\}_{m=1}^{N}$ of the damaged rod.

General results on the inverse Sturm–Liouville eigenvalue problem [23], [24] show that the full Dirichlet spectrum $\{\lambda_m\}_{m=1}^{\infty}$ is needed in order to have uniqueness. Therefore, since N is a finite number, our method will provide an estimate of the unknown coefficient p.

3 The identification method

Our identification method is of constructive type and is based on the following three main steps, which will be described in detail in the next subsections.

First step. The $(\widehat{p},\widehat{\rho})$-eigenvalue problem (1)–(2) is transformed into an impedance-type eigenvalue problem with coefficient $\widehat{A}$ by means of a Liouville transformation (see Section 3.1).

Second step. The theory of quasi-isospectral Sturm–Liouville operators in impedance form is applied to the eigenvalue problem for $\widehat{A}$ to construct a new impedance coefficient A which has the prescribed values of the first N eigenvalues of the damaged rod (see Section 3.2).

Third step. The Liouville transformation used in the First step is reversed to come back to a $(p,\widehat{\rho})$-eigenvalue problem of the type (6)–(7) and, therefore, to determine the axial stiffness p of the damaged rod (see Section 3.3).

3.1 Reduction to impedance-type form

We recall that the eigenvalue problem for the undamaged rod $(\widehat{p},\widehat{\rho})$ under Dirichlet end conditions is defined as follows

$$\frac{d}{dy}\left(\widehat{p}(y)\frac{dv(y)}{dy}\right) + \widehat{\lambda}\widehat{\rho}(y)v(y) = 0, \quad y \in (0,1)\,, \tag{10}$$

$$v(0) = 0 = v(1)\,. \tag{11}$$

Under our assumptions on the coefficients $\widehat{p}$ and $\widehat{\rho}$, we can apply the Liouville transformation

$$x = \psi(y) = \frac{1}{\widehat{M}}\int_0^y \sqrt{\frac{\widehat{\rho}(s)}{\widehat{p}(s)}}ds, \quad y \in [0,1], \tag{12}$$

$$\widehat{M} = \int_0^1 \sqrt{\frac{\widehat{\rho}(s)}{\widehat{p}(s)}}ds, \tag{13}$$

$$\widehat{A}(x) = \sqrt{\widehat{\rho}(y)\widehat{p}(y)}, \tag{14}$$

$$u(x) = v(y), \tag{15}$$

to reduce the problem (10)–(11) to the *impedance-type* eigenvalue problem

$$\frac{d}{dx}\left(\widehat{A}(x)\frac{du(x)}{dx}\right) + \widehat{\mu}\widehat{A}(x)u(x) = 0, \quad x \in (0,1)\,, \tag{16}$$

$$u(0) = 0 = u(1)\,, \tag{17}$$

where

$$\widehat{\mu} = \widehat{\lambda}\widehat{M}^2\,, \tag{18}$$

and

$$\widehat{A} \in C^2([0,1]), \quad \widehat{A}(x) \ge \sqrt{\alpha_0\beta_0} > 0 \quad \text{in } [0,1], \tag{19}$$

$$\widehat{A}(x) = \widehat{A}(1-x) \quad \text{in } [0,1]. \tag{20}$$

The application of the Liouville transformation (12)–(15) to equation (10) is standard. Regularity and uniform positivity conditions (19) easily follow from the corresponding properties of the coefficients $\widehat{p}$ and $\widehat{\rho}$. Let us check (20). By the symmetry of $\widehat{p}$ and $\widehat{\rho}$ we have

$$\begin{aligned}\widehat{A}(x) &= \widehat{A}(\psi(y)) = \sqrt{\widehat{\rho}(1-y)\widehat{p}(1-y)} \\ &= \widehat{A}(\psi(1-y))\,.\end{aligned} \tag{21}$$

Observing that

$$\begin{aligned}\psi(1-y) &= \frac{1}{\widehat{M}}\left(\int_0^1 \sqrt{\frac{\widehat{\rho}(s)}{\widehat{p}(s)}}ds - \int_{1-y}^1 \sqrt{\frac{\widehat{\rho}(s)}{\widehat{p}(s)}}ds\right) \\ &= 1 - \frac{1}{\widehat{M}}\int_0^y \sqrt{\frac{\widehat{\rho}(s)}{\widehat{p}(s)}}ds = 1 - \psi(y) \\ &= 1 - x\,,\end{aligned} \tag{22}$$

by (21) we obtain (20).

3.2 Impedance-type operators with given natural frequencies

In this section, starting from the impedance problem (16)–(17) with coefficient $\widehat{A} = \widehat{A}(x)$ satisfying (19)–(20) and having eigenvalues $\{\widehat{\mu}_m = \widehat{\lambda}_m \widehat{M}^2\}$, $m \geq 1$, we determine a new coefficient $A = A(x)$ such that the problem

$$\frac{d}{dx}\left(A(x)\frac{du(x)}{dx}\right) + \mu A(x)u(x) = 0, \quad x \in (0,1)\,, \quad (23)$$

$$u(0) = 0 = u(1)\,, \quad (24)$$

has exactly the first N eigenvalues

$$\mu_m = \lambda_m \widehat{M}^2, \quad m = 1, ..., N. \quad (25)$$

Here, $\{\lambda_m\}_{m=1}^N$ are the target eigenvalues of the damaged rod $(p, \widehat{\rho})$. We shall require that $A(x)$ satisfy the following conditions:

$$A \in C^2([0,1]), \quad A(x) \geq \gamma_0 > 0 \quad \text{in } [0,1], \quad (26)$$

$$A(x) = A(1-x) \quad \text{in } [0,1], \quad (27)$$

where γ_0 is a positive constant.

An explicit reconstruction of $A(x)$ with the above properties has been fully described in [6]. Referring to the Appendix for the essential details of the method, in the sequel we simply recall the main idea of the procedure. The key point is the explicit determination of a new impedance coefficient, say $A^*(x)$, such that the corresponding Dirichlet problem has exactly all the eigenvalues $\{\widehat{\mu}_m\}_{m=1}^\infty$ as the initial coefficient $\widehat{A}(x)$ in (16)–(17), with the exception of the nth eigenvalue, where n is a given integer, $n \geq 1$. We say that this impedance coefficient $A^*(x)$, or its associated impedance operator $\frac{1}{A^*(x)}\frac{d}{dx}\left(A^*(x)\frac{d}{dx}\right)$, is *quasi-isospectral* to $A(x)$ (respectively, to $\frac{1}{\widehat{A}(x)}\frac{d}{dx}\left(\widehat{A}(x)\frac{d}{dx}\right)$). Under the present assumptions on $\widehat{A}(x)$, the coefficient $A^*(x)$ turns out to be C^2-smooth, uniformly positive in $[0,1]$ and symmetric with respect to the mid-point $x = \frac{1}{2}$. The determination of $A^*(x)$ is based on a double application of a classical result of Analysis called Darboux's Lemma [11], which allows to find a closed-form expression for $A^*(x)$. Finally, by keeping fixed all the eigenvalues $\widehat{\mu}_m$ with $m \neq n$ and moving the nth eigenvalue $\widehat{\mu}_n$ to the desired value μ_n, and using repeatedly the procedure, after N steps one can determine a C^2-smooth, uniformly positive and even coefficient $A(x)$ with the first N given Dirichlet eigenvalues $\{\lambda_m\}_{m=1}^N$ of the damaged rod.

It should be noted that the coefficients $A(x)$ and $cA(x)$, where c is a positive constant, have the same spectrum. Therefore, in order to guarantee uniqueness of the reconstruction, one additional scalar information will be prescribed on $p(x)$ in the next step of the procedure.

3.3 Reconstruction of the damaged rod

We reverse the Liouville transformation (12)–(15) to write the eigenvalue impedance problem (23)–(24), with $A(x)$ satisfying (26)–(27) and such that (25) holds, into the eigenvalue problem for the supported rod with mass density $\widehat{\rho}$ (coinciding with the mass density of the undamaged rod) and with smooth, uniformly positive and even axial stiffness p, such that the first N eigenvalues of the rod $(p, \widehat{\rho})$ coincide with those prescribed for the damaged rod. Hereinafter, by even function in $[0,1]$ we mean even function with respect to the mid-point of the interval $[0,1]$.

Let us define

$$x = \phi(z) = \frac{1}{Q}\int_0^z f(s)ds, \quad z \in [0,1], \quad (28)$$

$$f(s) = \sqrt{\frac{\rho(s)}{\wp(s)}}, \quad (29)$$

$$Q = \int_0^1 f(s)ds, \quad (30)$$

$$A(x) = \sqrt{\rho(z)\wp(z)}, \quad (31)$$

$$u(x) = v(z), \quad (32)$$

where $\rho = \rho(z)$, $\wp = \wp(z)$ are unknown functions which must satisfy the conditions

$$\rho, \wp \in C^2([0,1])\,, \quad \rho(z) \geq \delta_0 > 0\,,$$
$$\wp(z) \geq \epsilon_0 > 0\,, \text{in } [0,1]\,, \quad (33)$$

$$\wp(z) = \wp(1-z), \quad \rho(z) = \rho(1-z) \quad \text{in } [0,1], \quad (34)$$

with δ_0, ϵ_0 suitable positive constants. By applying the transformation (28)–(32), the eigenvalue problem (23)–(24) becomes

$$\frac{d}{dz}\left(Q\wp(z)\frac{dv(z)}{dz}\right) + \lambda\frac{\widehat{M}^2}{Q}\rho(z)v(z) = 0\,, \quad (35)$$

$$v(0) = 0 = v(1)\,, \quad z \in (0,1) \quad (36)$$

where the definition $\mu = \lambda\widehat{M}^2$ has been used. Let us replace the quantity $\frac{\widehat{M}^2}{Q}\rho(z)$ with the mass density of the undamaged rod, that is, let us assume

$$\rho(z) = \frac{Q}{\widehat{M}^2}\widehat{\rho}(z) \quad \text{in } [0,1], \quad (37)$$

so that the mass density of the rod is unchanged. Note that, by (37), the function $\rho = \rho(z)$ is a C^2-regular, uniformly positive and even function in $[0,1]$.

To conclude the construction, we need to determine the function $Q\wp(z)$ in (35) or, equivalently, the function $f = f(z)$. Using (37) in (31), and multiplying both sides

of (31) by $f(z)$, we obtain the following equation in the unknown $f(z)$:

$$\widehat{M}^2 A\left(\frac{1}{Q}\int_0^z f(s)ds\right)\frac{f(z)}{Q}=\widehat{\rho}(z),\quad \text{in } [0,1], \tag{38}$$

where $\widehat{M}$, $\widehat{\rho}(z)$ are known quantities, and the function $A=A(x)$, $x\in[0,1]$, has been determined in Section 3.2.

We first prove that a solution to (38), if any, is an even function in $[0,1]$. To show this property, noticing that $\int_0^1 f(1-s)ds=\int_0^1 f(s)ds$, it is enough to prove that if $f(z)$ solves (38), then also $f(1-z)$ solves (38), that is

$$\widehat{M}^2 A\left(\frac{1}{Q}\int_0^z f(1-s)ds\right)\frac{f(1-z)}{Q}=\widehat{\rho}(z),\quad \text{in } [0,1]. \tag{39}$$

Putting $\zeta=1-z$ in (39), recalling that $\widehat{\rho}(1-z)=\widehat{\rho}(z)$ in $[0,1]$, and using again (38) to express $\widehat{\rho}(\zeta)$, condition (39) can be written as

$$A\left(\frac{1}{Q}\int_0^{1-\zeta} f(1-s)ds\right)=A\left(\frac{1}{Q}\int_0^{\zeta} f(s)ds\right),$$
$$\zeta\in[0,1]. \tag{40}$$

Let us elaborate the left hand side of (40). By introducing the change of variables $t=1-s$ and recalling that $A(x)$ is an even function in $[0,1]$ (see (27)), we have

$$A\left(\frac{1}{Q}\int_0^{1-\zeta} f(1-s)ds\right)=A\left(\frac{1}{Q}\int_\zeta^1 f(t)dt\right)$$
$$=A\left(1-\frac{1}{Q}\int_0^{\zeta} f(t)dt\right)=A\left(\frac{1}{Q}\int_0^{\zeta} f(t)dt\right), \tag{41}$$

and (40) is satisfied. Moreover, since $A(x)$ is an even function in $[0,1]$, if $f(z)$ is an even function in $[0,1]$, then also $A\left(\frac{1}{Q}\int_0^\zeta f(t)dt\right)$ is an even function of z in $[0,1]$.

To solve (38) we found convenient to put

$$\eta'(z)=\frac{f(z)}{Q},\quad \text{in } [0,1], \tag{42}$$

that is

$$\eta(z)=\eta(0)+\frac{1}{Q}\int_0^z f(s)ds,\quad \text{in } [0,1], \tag{43}$$

where $\eta(0)$ is an integration constant. Let

$$\overline{\eta}(z)=\eta(z)-\eta(0). \tag{44}$$

Then $\overline{\eta}'(z)=\eta'(z)$ in $(0,1)$ and the function $\overline{\eta}$ solves the equation

$$\widehat{M}^2 A(\overline{\eta}(z))\overline{\eta}'(z)=\widehat{\rho}(z),\quad \text{in } (0,1). \tag{45}$$

Since f is an even function, we have

$$\overline{\eta}\left(\frac{1}{2}\right)=\frac{\int_0^{\frac{1}{2}} f(s)ds}{\int_0^1 f(s)ds}=\frac{1}{2} \tag{46}$$

and $\overline{\eta}(z)$ solves the Cauchy's problem

$$\overline{\eta}'(z)=\frac{\widehat{\rho}(z)}{\widehat{M}^2 A(\overline{\eta}(z))},\quad z\in\left(\frac{1}{2},1\right), \tag{47}$$

$$\overline{\eta}\left(\frac{1}{2}\right)=\frac{1}{2}. \tag{48}$$

Under our assumptions on the coefficients, there exists a unique regular solution to (47)–(48) in $\left[\frac{1}{2},1\right]$. The solution can be determined numerically, as explained in Section 4.3. Recalling that $\overline{\eta}'=\eta'$ in $(0,1)$, the function $\overline{f}(z)=\frac{f(z)}{Q}$ $(=\eta'(z))$ is known in $\left[\frac{1}{2},1\right]$. Since $f(z)$ is even in $[0,1]$, we can extend $\overline{f}(z)$ (and, therefore, $\overline{\eta}'(z)$) to the whole interval $[0,1]$ evenly with respect to $z=\frac{1}{2}$, that is $\overline{f}(z)$ (and, therefore, $\overline{\eta}'(z)$) is known in $[0,1]$. It should be noticed that, in order to simplify the notation, we simply indicate by $\overline{f}$, $\overline{\eta}'$ the extension of $\overline{f}$, $\overline{\eta}'$, respectively.

We are now in position to evaluate the stiffness coefficient $Q\wp(z)$ appearing on the first term of the right hand side of (35). By the definition of $\overline{\eta}(z)$, and using (29) and (37), we have

$$\overline{\eta}'(z)=\frac{1}{Q}\sqrt{\frac{\rho(z)}{\wp(z)}}=\frac{1}{Q}\frac{\sqrt{Q\widehat{\rho}(z)}}{\widehat{M}\sqrt{\wp(z)}}=\frac{\sqrt{\widehat{\rho}(z)}}{\widehat{M}\sqrt{Q\wp(z)}}, \tag{49}$$

and, finally,

$$p(z)\equiv Q\wp(z)=\frac{\widehat{\rho}(z)}{\widehat{M}^2(\overline{\eta}'(z))^2},\quad \text{in } [0,1]. \tag{50}$$

The function $p(z)$ is of C^2-class, uniformly positive in $[0,1]$, and even with respect to $z=\frac{1}{2}$. This concludes the determination of the function $p(z)$.

As it was mentioned at the end of Section 3.2, the impedance coefficients $A(x)$ and $cA(x)$ have the same full Dirichlet spectrum for any positive value of the constant c. It can be shown that this indeterminacy does not affect Equation (35). On the contrary, if we replace $A(x)=\sqrt{\rho(z)\wp(z)}$ by $A(x)=c\sqrt{\rho(z)\wp(z)}$ in (31), then a multiplicative factor c appears on the left hand side of (45), and the axial stiffness $p(z)$ in (50) becomes $c^2p(z)$. The indeterminacy on $A(x)$, and, consequently, on $p(z)$, can be removed by assigning an additional scalar information on the axial stiffness. The integral of the axial stiffness $p(z)$ on the whole rod axis interval $[0,1]$, $\int_0^1 p(x)dx$, has been prescribed in all the numerical simulations performed in the sequel. No difference was noticed in the results of the reconstruction by prescribing the integral of the inverse of the axial stiffness $p(z)$ on

$[0,1]$. Alternative point-wise information on the axial stiffness coefficient were also investigated, see Section 5.2.3.

4 Reconstruction algorithm

This section is devoted to the numerical implementation of the identification method described in Section 3. In particular, the main numerical tools are described in the next subsections.

4.1 High-Continuity finite element approximation

The weak formulation of the eigenvalue problem (6)–(7) consists in finding $v \in H_0^1(0,1) \setminus \{0\}$ and $\lambda \in \mathbb{R}^+$ such that

$$\int_0^1 pv'\varphi' = \lambda \int_0^1 \widehat{\rho} v\varphi, \quad \text{for every } \varphi \in H_0^1(0,1). \tag{51}$$

The functions p and $\widehat{\rho}$ are assumed to satisfy the conditions (3)–(4) (with $\widehat{\rho}$ replaced by p). Here, $H_0^1(0,1)$ is the Hilbert space of Lebesgue measurable functions $f : (0,1) \to \mathbb{R}$ such that f and its first weak derivative f' are square integrable in $(0,1)$, *e.g.* $\|f\|^2_{H^1(0,1)} = \int_0^1 (f^2 + (f')^2) < \infty$, and the trace of f at $x = 0$ and $x = 1$ vanishes, *e.g.*, $f(0) = f(1) = 0$.

To find a discrete version of Eq. (51) we work on the finite dimensional subspace $\mathcal{H}$, $\mathcal{H} \subset H^1(0,1)$, of the second order B-spline test functions, see [34] for a general introduction on B-splines. It can be shown that this class of test functions allows to obtain very refined results with computational cost similar to that of piecewise linear interpolation. We refer, among other contributions, to [2,5] for more details on second order B-spline interpolation in finite element analysis in two- and three-dimensional problems. The one-dimensional case used in the present work can be easily derived from [3,41]. In brief, the explicit expression of the three test functions on a generic interior eth finite element is

$$\mathbf{\Phi}_e(\xi) = \begin{bmatrix} \frac{1}{8}(1 - 2\xi + \xi^2) \\ \frac{1}{4}(3 - \xi^2) \\ \frac{1}{8}(1 + 2\xi + \xi^2) \end{bmatrix}, \tag{52}$$

where ξ belongs to the normalized interval $[-1,1]$. Specific test functions are chosen in the first (near $x = 0$) and last (near $x = 1$) finite element of the mesh, see again [5]. The unknown function v can be approximated within the eth finite element by the function $\widetilde{v}_e$ given by

$$\widetilde{v}_e = \mathbf{\Phi}_e^T \widetilde{\mathbf{v}}_e \,, \tag{53}$$

where $\mathbf{\Phi}_e^T$ is the row vector containing the test functions and $\widetilde{\mathbf{v}}_e$ is the vector of the nodal axial displacements. Therefore, the discrete version of Eq. (51) consists in solving the finite dimensional eigenvalue problem

$$\mathbf{K}\widetilde{\mathbf{v}} = \widetilde{\lambda}\mathbf{M}\widetilde{\mathbf{v}} \,, \tag{54}$$

where $(\widetilde{\lambda}, \widetilde{\mathbf{v}})$ is the approximation of the continuous eigenpair (λ, v). The global stiffness and inertia matrices $\mathbf{K}$ and $\mathbf{M}$ are obtained by means of a standard finite element procedure of assemblage of the local matrices $\mathbf{K}_e = \int_{-1}^1 p\, \mathbf{\Phi}'_e \mathbf{\Phi}'^T_e J \,\mathrm{d}\xi$ and $\mathbf{M}_e = \int_{-1}^1 \widehat{\rho}\, \mathbf{\Phi}_e \mathbf{\Phi}_e^T J \,\mathrm{d}\xi$, where the Jacobian J correlates normalized and physical spatial coordinates. The integrals were evaluated numerically by means of a 8-point Gaussian quadrature rule, which gives exact results for polynomials up to the 15th degree. In spite of the fact that test functions are quadratic, the choice of such high degree turns out to be suitable in our problem, since the reconstructed axial stiffness p typically is an highly oscillating function, as it will be shown in Section 5. The discrete eigenvalue problem (54) has been solved using the MatLab routine *eig*, which is based on the QZ algorithm [17].

4.2 Evaluation of the fundamental solutions

As it was recalled in Section 3.2, the determination of the impedance coefficient $A(x)$ in (23)–(24) requires a repeated use of (107). Application of (107), in turn, requires the determination of the fundamental solutions y_1, y_2 defined in Eqs. (95)–(97), (98)–(100), respectively; see the Appendix. The calculation of y_i, $i = 1,2$, is briefly described in the present subsection. The interested reader is referred to the paper [6] for a comprehensive treatment of the numerical aspects.

We recall that, for a fixed value of the real parameter λ, the fundamental solutions y_i are solutions of the initial value problem

$$y'' + \lambda y = qy \,, \qquad x \in (0,1) \,, \tag{55}$$

$$y(0) = y_0 \,, \tag{56}$$

$$y'(0) = \dot{y}_0 \,, \tag{57}$$

with $(y_0 = 1,\ \dot{y}_0 = 0)$ and $(y_0 = 0,\ \dot{y}_0 = 1)$ for $i = 1,2$, respectively. The Schrödinger potential $q \in C^0([0,1])$ is defined as $q(x) = \frac{a''(x)}{a(x)}$. The initial value problem (55)–(57) has been solved via the Stoermer's method [12]. By considering a grid of equally spaced points of the interval $[0,1]$, say $\{x_j\}_{j=0}^P$, with $x_0 = 0$, $x_j = x_0 + jH$, $j = 1, \cdots, P$ and $H = \frac{1}{P}$, the Schrödinger potential q has been estimated in each interior point x_i, $1 \le i \le$

$P-1$, by using the central finite difference formula to approximate the second derivative of $a(x)$:

$$a''(x_i) \simeq \frac{a_{i-1} - 2a_i + a_{i+1}}{H^2}\,, \tag{58}$$

where $a_i = a(x_i)$ and, therefore, $q(x_i) = \frac{a''(x_i)}{a(x_i)}$. The use of approximation (58) produces an error of order H^2. Suitable expressions of the second derivative of the function $a = a(x)$ have been chosen at the beginning and at the end of the grid in order to ensure the same degree of accuracy of the approximation; see [6] (Section 3) for more details.

Denoting by $\{y_j\}_{j=0}^P$ the approximate solution to Eq. (55) at the points $\{x_j\}_{j=0}^P$, *e.g.*, $y(x_j) \simeq y_j$, the Stoermer's integration scheme is based on a further subdivision in m parts of length $h = \frac{H}{m}$ of each interval (x_j, x_{j+1}). Let us denote by $\{x_{j_k}\}_{k=0}^m$ the points of the sub-grid, with $x_{j_k} = x_{j_0} + kh$, $k = 0, \cdots, m$, $x_{j_0} = x_j$ and $x_{j_m} = x_{j+1}$. Moreover, let $y_{j_k} = y(x_{j_k})$ and $y'_{j_k} = y'(x_{j_k})$. The second derivative of y at the points $\{x_{j_k}\}_{k=1}^{m-1}$ is estimated as

$$y''(x_{j_k}) \simeq \frac{y_{j_{k+1}} - 2y_{j_k} + y_{j_{k-1}}}{h^2} = (q_{j_k} - \lambda) y_{j_k}\,,$$
$$k = 1, \cdots, m-1\,. \tag{59}$$

As before, suitable expressions based on parabolic extrapolation are adopted for estimating the value of y at the first point, x_{j_1}, and at the last point, x_{j_m}, of the grid. The integration scheme was coded following the procedure sketched in Table 1 and due to Henrici [22].

The number of subdivisions of each grid interval can be chosen freely, even if, as it was suggested in [12,18], an even value of m improves the numerical efficiency. In all the numerical test reported below we have set $m = 2$.

4.3 Cauchy's problem solution

The third step of the damage reconstruction algorithm requires the solution of Cauchy's problem (47)–(48). Here, the presence of a first order differential equation suggests the use of an integration scheme based on the trapezium rule. The integration of (47) leads to

$$\overline{\eta}(z) - \frac{1}{2} = \int_{\frac{1}{2}}^{z} g(\tau, \overline{\eta}(\tau)) \mathrm{d}\tau\,, \tag{60}$$

where

$$g(z, \overline{\eta}(z)) = \frac{\widehat{\rho}(z)}{\widehat{M}^2 A(\overline{\eta}(z))}\,, \quad z \in [0,1]\,. \tag{61}$$

Let N_e be an even number. We introduce a uniform subdivision of the interval $(\frac{1}{2}, 1)$ in $N_e/2$ points $\{z_n\}_{n=0}^{N_e/2}$ such that $z_{n+1} = z_n + h$, with $h = \frac{1}{N_e}$, and we denote by $\overline{\eta}_n$ the approximation of the solution $\overline{\eta} = \overline{\eta}(z)$ of (47)–(48) at $z = z_n$, $n = 0, ..., N_e/2$. Using the Crank–Nicolson method we have

$$\overline{\eta}_{n+1} = \overline{\eta}_n + \frac{h}{2}(g_n + g_{n+1})\,, \tag{62}$$

where $g_n = g(z_n, \overline{\eta}(z_n))$. The recursive formula (62) is of implicit type, since it requires the evaluation of g_{n+1}. Two methods have been implemented to solve numerically (62). The first one consists in the transformation of the implicit integration scheme in an explicit one by replacing g_{n+1} with $g(z_{n+1}, \overline{\eta}_n + hg_n)$ via the explicit Euler-forward method, usually named Heun's method (see [17] for more details):

$$\overline{\eta}_{n+1} = \overline{\eta}_n + \frac{h}{2}\left(g_n + g(t_{n+1}, \overline{\eta}_n + hg_n)\right). \tag{63}$$

The second scheme is based on the fixed point iteration method

$$\overline{\eta}_{n+1}^{(k+1)} = \overline{\eta}_n^{(k)} + \frac{h}{2}(g_n^{(k)} + g_{n+1}^{(k)})\,, \tag{64}$$

being k the iteration index. In order to estimate $\overline{\eta}_{n+1}^{(0)}$, we can use again the Euler explicit approximation, *i.e.* $\overline{\eta}_{n+1}^{(0)} = \overline{\eta}_n + hg_n$, where $\overline{\eta}_n$ and g_n are known from the previous step.

For a given value of the step-length $h = 1/N_e$, $N_e = 1600$, the results obtained by the integration schemes (63) and (64) were practically the same. For the sake of definiteness, Heun's method will be adopted in the sequel.

5 Reconstruction results

In this Section we present the results of an extended series of numerical applications. Among other parameters, the sensitivity of the identification procedure has been tested with respect to the number N of the first eigenfrequencies used and to the geometry of the damage (*e.g.*, position, severity and local character of the damage). The ability of the method in detecting multiple damages and the effect of additional scalar information on the inverse reconstruction problem have been also investigated. The first part of the section deals with free-error data, *i.e.*, the measurement errors are null with the exception of the errors induced by the numerical approximation. The stability of the method in presence of noise is evaluated in Section 5.3. All the results refer to an initially *undamaged* uniform rod under supported end conditions, with $L = 1$, $\widehat{p}(x) = 1$ and $\widehat{\rho}(x) = 1$ in $[0,1]$.

Table 1 Henrici's algorithm to compute fundamental solutions.

Prime	$\Delta_0 = hy'_{j_0} + \frac{1}{2}h^2(q_{j_0} - \lambda)y_{j_0}$
	$y_{j_1} = y_{j_0} + \Delta_0$
Repeat for $k = 1, \cdots, m-1$	$\Delta_k = \Delta_{k-1} + h^2(q_{j_k} - \lambda)y_{j_k}$
	$y_{j_{k+1}} = y_{j_k} + \Delta_k$
Set	$y'_{j_m} = \dfrac{\Delta_{m-1}}{h} + \frac{1}{2}h\left(q(x_0 + H) - \lambda\right) y_{j_m}$

5.1 Damage modelling

The method has been tested on a class of damaged rods containing either single or multiple localized damages. Each damage is described as a smooth stiffness reduction with support coinciding with a closed interval compactly contained in $[0, 1]$. More precisely, the typical damage profile is designed by using a 5th order Bézier curve with 6 control points, see Figure 1, in such a way to satisfy C^2 regularity of the axial stiffness $p(x)$. Geometrical parameters are the position b along the rod axis, the (half) extension c of the damaged region, and the maximum stiffness reduction e.

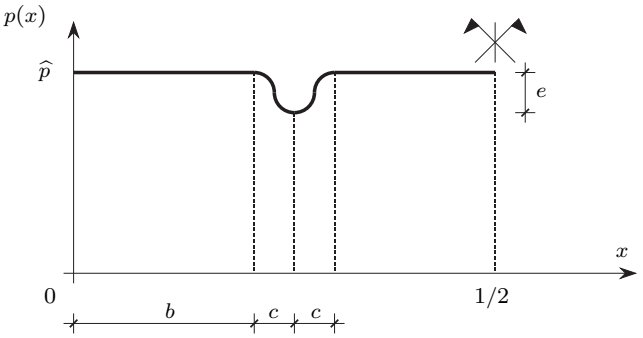

(a) Geometric damage parameters

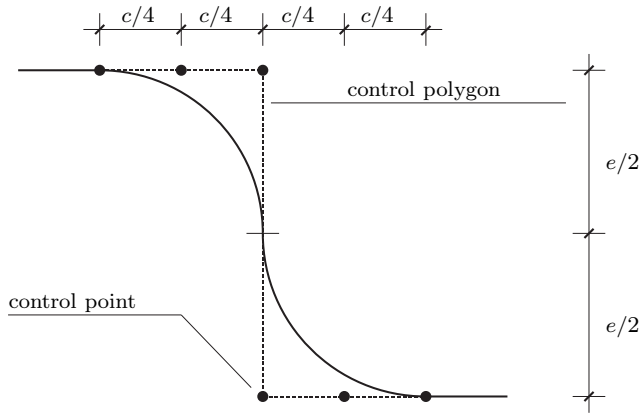

(b) Bézier representation of the stiffness profile (left joint)

Fig. 1 Geometry of the damage and Bézier modelling.

We recall that a 5th-order Bézier curve is defined as

$$\mathbf{C_5}(\xi) = \sum_{i=0}^{5} B_{i,5}(\xi)\,\mathbf{P}_i\,, \qquad 0 \le \xi \le 1\,, \tag{65}$$

where $B_{i,5}(\xi)$ are the 5th-degree blending functions (*i.e.*, 5th-degree Bernstein's polynomials) and $\mathbf{P}_i$ are the control points, see Table 2. We refer to the book [34] for a in-depth treatment of Bézier curves or to [8] for a quick introduction on the same issue.

It should be noticed that our choice allows to study a wide class of rod profiles, including the cases of small/severe and localized/diffuse damage. Among a large number of simulations, attention will be mainly focussed on the most challenging and difficult cases, which correspond to small stiffness reduction concentrated in few small intervals, that is both the parameters c and e are chosen to be small. The analysis of these situations allows to check the sensitivity of the method to the identification of the damage just as it arises in the bar. In particular, reference is typically made to the presence of a single damage (in each half of the rod) with $c = 0.025$ and $e = 0.20 - 0.40$, namely the maximum stiffness reduction is about $20 - 40\%$ of the reference value and the extension of the damaged region is 5% of the total length of the rod. Damages belonging to this class can be considered *small damages*, since the percentage variation is of order $1 - 3\%$ for the first thirty natural frequencies.

In order to select a suitable mesh for the numerical solution of the eigenvalue problem (54), we firstly considered the free vibration of a uniform rod. In this case, natural frequencies can be computed analytically and therefore the selection of a mesh producing an error less than a fixed cut-off is simple. For example, if we consider $N_e = 100$ equally spaced finite elements, than the maximum error on the first 30 frequencies is 0.13%. In case of nonuniform rods, no closed form reference solution is generally available. For this reason, we considered a sequence of increasingly refined meshes having $N_e = sr^k$ finite elements, where $r = 2$ and $s = 400$, $k = 1, 2, 3, \cdots$. As error indicator we choose the expression

$$E_N = \left(\sum_{i=1}^{N} \left(\frac{f_i}{i/2} - 1 \right)^2 \right)^{\frac{1}{2}}, \tag{66}$$

Table 2 Blending functions $B_{i,5}$ and control points $P_i^{(L)}$ (left joint) and $P_i^{(R)}$ (right joint), see Fig. 1(b), for 5th-order Bézier curve.

	i					
	0	1	2	3	4	5
$B_{i,5}$	$(1-\xi)^5$	$5\xi(1-\xi)^4$	$10\xi^2(1-\xi)^3$	$10\xi^3(1-\xi)^2$	$5\xi^4(1-\xi)^2$	ξ^5
$P_i^{(L)}$	$(b,\widehat{p})$	$(b+\frac{1}{4}c,\widehat{p})$	$(b+\frac{1}{2}c,\widehat{p})$	$(b+\frac{1}{2}c,\widehat{p}-e)$	$(b+\frac{3}{4}c,\widehat{p}-e)$	$(b+c,\widehat{p}-e)$
$P_i^{(R)}$	$(b+c,\widehat{p}-e)$	$(b+\frac{5}{4}c,\widehat{p}-e)$	$(b+\frac{3}{2}c,\widehat{p}-e)$	$(b+\frac{3}{2}c,\widehat{p})$	$(b+\frac{7}{4}c,\widehat{p})$	$(b+2c,\widehat{p})$

having denoted by $f_i = \frac{\sqrt{\lambda_i}}{2\pi}$ and $\frac{i}{2}$ the ith natural frequency of the damaged rod and the uniform rod, respectively, and by N the number of considered frequencies. The error indicator E_{30} for increasing N_e, and for the case with $b = 0.24$, $c = 0.025$ and $e = 0.2$, is reported in Fig. 2. The following deductions can be made from the analysis of this figure: (i) meshes corresponding to $N_e = 3200$, 6400 and 12800 produce approximately the same value of E_{30}, being their differences less than 10^{-5}, therefore, the results obtained by $N_e = 12800$ can be retained as reference solution and the corresponding mesh is indicated as *refined* mesh in what follows; (ii) the mesh with $N_e = 1600$ is a good compromise between accuracy (E_{30} differs of about 0.004% with respect to the refined mesh) and computational cost. This mesh will be used to perform all the following numerical simulations, and it will be denoted as *working* mesh. Finally, all the target natural frequencies are assigned in ascending order, from the first to the Nth, see [6] (Section 4.6).

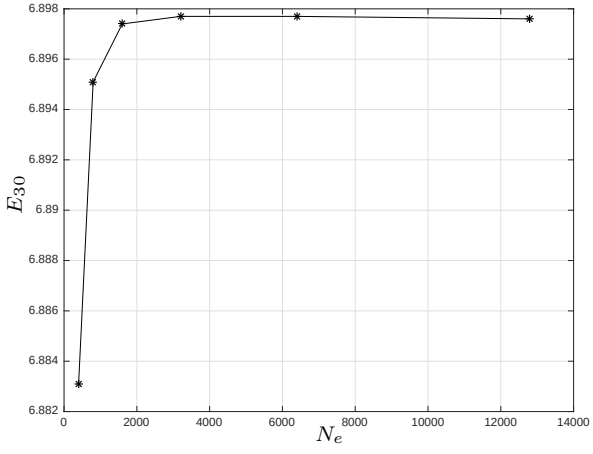

Fig. 2 Error indicator E_{30} versus the number of finite elements N_e.

5.2 Applications to free-error data

5.2.1 Influence of the number of eigenfrequencies

The influence of the number of eigenfrequencies on the results of identification is initially investigated. The profiles shown in Figure 3 have been obtained for single damage, with $b = 0.24$, $c = 0.025$ and $e = 0.2$, varying the number N from 5 to 30. In all the plots of this figure, and also in the figures below, we used the following notation: thick black and thin red curves represent the exact and the reconstructed normalized stiffness coefficient $p(x)/\widehat{p}$, respectively. Furthermore, the eigenfrequency percentage shifts induced by the damage on the initially uniform rod are collected at the top of each sub-figure, *i.e.* $\delta_m = 100 \times (f_m^{\rm dam} - f_m^{\rm uni})/f_m^{\rm uni}$, $m = 1, ..., N$. The differences between computed (after the reconstruction) and target eigenfrequencies are shown on the bottom, *i.e.* $\rho_m = 100 \times (f_m^{\rm rec} - f_m^{\rm tar})/f_m^{\rm tar}$.

The analysis of Figure 3 shows that the accuracy of the reconstruction generally improves as N increases. More precisely, a low number of eigenfrequencies (up to $N = 10$, say) allows to recover an "averaged" behavior of the unknown coefficient $p(x)$ only, whereas accurate pointwise L^∞-estimates require the first $15-20$ eigenfrequencies. The above considerations are rigorously true in the whole interval $[0, 1]$ with the exception of points close to the ends of the rod. These end neighborhoods contain spurious fluctuations of the reconstructed coefficient p. The fluctuations attain the minimum reduction exactly at the ends of the rod, and their amplitude decays in oscillatory manner proceeding toward the mid-point of the rod. Moreover, from Figure 3 it can be noticed that value $p(0)$ decreases as the number N increases. This trend seems to be a typical feature of the reconstruction method and, in some cases, may obstruct the correct identification, especially in case of damages located near the ends of the rod.

It should be also noticed that the results of numerical simulations, not reported here for brevity, show that the accuracy of the reconstruction does not improve significantly by taking N larger than $30 - 40$. In fact, the following eigenvalue asymptotic formula holds as

$m \to \infty$ (see [24]):

$$\sqrt{\lambda_m} = \frac{m\pi}{M} + O\left(\frac{1}{m}\right), \tag{67}$$

where $M = \int_0^1 \sqrt{\frac{\widehat{\rho}(s)}{p(s)}} ds$ and $C > 0$ is a constant independent from m such that $\left|O\left(\frac{1}{m}\right)\right| \leq \frac{C}{m}$ for m large enough. Formula (67) shows that higher eigenvalues contain information essentially on the "average-type" quantity M rather than on the point-wise values of $p(x)$. Moreover, from (67) and its analogue for the undamaged rod, it can be shown that

$$\delta_m = \frac{\widehat{M} - M}{M} + O\left(\frac{1}{m^2}\right), \quad \text{as m } \to \infty, \tag{68}$$

that is the eigenfrequency percentage shifts δ_m induced by the damage are asymptotically equal to a negative constant, as the histogram placed at the top of each sub-figure in Figure 3 shows.

We conclude this subsection by presenting a justification of the wavy boundary layer behavior of the reconstructed axial stiffness coefficient. Let us evaluate the coefficient $A(x)$ in (23) at $x = 0$ or, equivalently, at $x = 1$. A direct calculation via (107) shows that, starting from the uniform rod $\widehat{\rho} = \widehat{p} = 1$ and imposing the first N eigenvalues $\{\mu_m\}_{m=1}^N$ of the damaged rod, we have

$$A(0) = \left(\prod_{m=1}^{N} \frac{\mu_m}{\widehat{\mu}_m}\right)^2. \tag{69}$$

From expression (69) we can infer that:

i) $A(0)$ may be significantly less than the unit value, since $\mu_m < \widehat{\mu}_m$ for every $m \geq 1$ by Monotonicity Theorems (see, for example, [10]);

ii) $A(0)$ is a decreasing function of N.

Moreover, on assuming that the reconstructed axial stiffness coefficient tends to the target profile as $N \to \infty$, an oscillatory character of the reconstructed coefficient is naturally expected near the ends of the rod to connect the end value, which can be significantly less than 1, to the unit value inside the undamaged portion of the rod. For the sake of completeness, it should be noticed that the wavy character of the reconstructed coefficient was also encountered in the determination of blockages in an acoustic duct via quasi-isospectral horn operators [6], for which the expression (69) continues to hold. However, the effects found in [6] were much less important with respect to the present case, since for the horn equation the ratios $\frac{\mu_m}{\widehat{\mu}_m}$ may be less, equal or even bigger than 1, resulting on slight global deviation of $A(0)$ from the initial unit value.

5.2.2 Influence of the geometry of the damage

The influence of the damage profile is investigated in Figures 4–7. All the results refer to single damage in half of the rod, which the exception of Figure 7, which is devoted to multiple damages. The number N is always taken equal to 20.

The effect of different damage position is considered in Figure 4. In addition to $b = 0$ (*half* end damage), two values of b are considered, namely $b = 0.12$ and 0.36; the remaining damage parameters are $c = 0.025$ and $e = 0.2$. In all the cases the identification is successful.

Setting $b = 0.24$ and $c = 0.025$, the influence of damage severity is investigated in Figure 5 for $e = 0.1$, 0.2, 0.4. As expected, the wavy character of the reconstructed profile increases as the severity of the damage increases, and the spurious fluctuations propagate from the ends to the interior of the rod approximately up to the damaged region. An appreciable deterioration of the results starts to be evident from $e = 0.4$.

The results reported in Figure 6 refer to $b = 0.24$, $e = 0.2$ and to increasing values of the extension of the damaged region from $c = 0.025$ to $c = 0.1$, corresponding to localized and diffuse damage. Diffuse damage induces bigger reductions of the eigenfrequencies and, therefore, large reductions of the reconstructed axial stiffness are attained at the ends $x = 0$ and $x = 1$. As it was discussed above, the end oscillations become larger and larger, and tend to mask the correct localization of the damaged regions. The accuracy in damage quantification is almost compromised in case of large and diffuse damage, see Figure 6(c).

Figure 7 reports the damage reconstruction in case of two consecutive damages at distance βc, where β varies from 0 (adjacent damages, Figure 7(a)) to 4. It turns out that the method is able to separate close localized damages and also to correctly reconstruct adjacent damages.

5.2.3 Influence of the scaling factor

It has been noticed at the end of Section 3.2 that the axial stiffness $p(x)$ can be determined up to a multiplicative constant. In order to remove this indeterminacy, the a priori information on the scalar quantity $\int_0^1 p(x)dx$ has been included in the above analysis. Figure 8 compares the results obtained with and without this information. Numerical results confirm that the reconstruction is strongly influenced by scaling.

Other kinds of additional scalar information were experienced, such as the knowledge of $\int_0^1 p^{-1}(x)dx$ or the value of p at the mid-point of the rod. It is worth noticing that this latter information always resulted in

a final stiffness profile indistinguishable from that obtained by using the a priori knowledge of $\int_0^1 p(x)dx$, at least in cases in which - obviously - the mid-point $x = 1/2$ does not belong to the damaged region of the rod. This is a very usable result in practical applications, especially when the knowledge of $\int_0^1 p(x)dx$ (or $\int_0^1 p^{-1}(x)dx$) is not easily accessible.

5.2.4 Recovering unsymmetrical damage

General results on the inverse spectral theory for the Sturm-Liouville operator $(p, \widehat{\rho})$ in (6)–(7), with $\widehat{\rho}$ given function in $[0, 1]$, shows that the knowledge of the full Dirichlet spectrum does not determine uniquely a (smooth) unsymmetrical stiffness coefficient p. In spite of this, we have tested the capability of the method in recovering an unsymmetrical stiffness coefficient from the first N Dirichlet eigenfrequencies. The results for $b = 0.24$, $c = 0.025$, $e \in \{0.2, 0.4\}$ are shown in Figure 9. As expected, the reconstructed profile is symmetric and shows an appreciable reduction of the axial stiffness exactly inside the actual damaged area. The estimate of the damage severity, however, is rather inaccurate, showing an underestimate of about 50%.

5.3 Applications to noisy data

The sensitivity of a damage reconstruction algorithm to errors on the input data is an important issue. Denoting by f_m^{noise} the mth perturbed eigenfrequency, we have considered two classes of random noisy data, namely, for $m \geq 1$:

$$f_m^{\text{noise I}} = f_m + \eta f_1\,, \tag{70}$$

$$f_m^{\text{noise II}} = f_m(1 + \eta)\,, \tag{71}$$

where $\eta = \eta_{\max}(2r - 1)$ and r is a random number generated from a uniform distribution on the interval $[0, 1]$. The maximum error level is denoted by $\eta_{\max}$. In case of Equation (70), the maximum error level does not depend on the mode order m and, therefore, it can be attributed to measurement errors. On the contrary, in Equation (71), the maximum error increases (linearly) as the mode order increases, so describing possible modelling errors, since, as it is well known, the classical model of longitudinally vibrating rods we have adopted looses accuracy as the mode order increases.

Figures 10 and 11 report some illustrative examples of identification varying the error level $\eta_{\max}$ and the damage severity. Results are referred to $b = 0.24$, $c = 0.025$ and $N = 20$. The reconstruction turns out to be sufficiently stable and robust to errors of the type Eq. (70) up to $\eta_{\max} = 0.03$. Conversely, our simulations show that the effect of noise of the type Eq. (71) is larger, and the reconstruction is almost compromised for very small damages. In these cases, in fact, the eigenfrequency shifts induced by damage are comparable with the errors on the data, resulting on significant difficulty on damage identification.

6 An extension to Neumann end conditions

In this Section we show how the damage analysis developed above can be adapted to deal with rods under Neumann end conditions. The infinitesimal undamped vibration of the undamaged free-free rod $(\widehat{P}, \widehat{R})$ with unit length are governed by the eigenvalue problem

$$(\widehat{P}k')' + \widehat{\lambda}\widehat{R}k = 0, \quad \text{in } (0, 1)\,, \tag{72}$$

$$(\widehat{P}k')(0) = 0 = (\widehat{P}k')(1)\,, \tag{73}$$

where the axial stiffness $\widehat{P}$ and the mass density $\widehat{R}$ satisfy conditions (3)–(5), with $\widehat{p}$, $\widehat{\rho}$ replaced by $\widehat{P}$, $\widehat{R}$, respectively. The eigenvalues of (72)–(73) are $\{\widehat{\lambda}_m\}_{m=0}^{\infty}$, with $0 = \widehat{\lambda}_0 < \widehat{\lambda}_1 < \widehat{\lambda}_2 < ...$, $\lim_{m\to\infty} \widehat{\lambda}_m = \infty$. Under the assumptions of Section 2, the eigenvalue problem for the damaged rod is

$$(Pk')' + \lambda\widehat{R}k = 0, \quad \text{in } (0, 1)\,, \tag{74}$$

$$(Pk')(0) = 0 = (Pk')(1)\,, \tag{75}$$

where the axial stiffness P satisfies (3), (5) (with $\widehat{p}$ replaced by $\widehat{P}$) and the eigenvalues are $0 = \lambda_0 < \lambda_1 < \lambda_2 < ...$, $\lim_{m\to\infty} \lambda_m = \infty$. With the aim of determining the axial stiffness P from the knowledge of $\{\lambda_m\}_{m=1}^{N}$ (note that $\lambda_0 = 0$ is insensitive to damage), we recall the following simple, but useful result: all the positive eigenvalues of (72)–(73) coincide with the eigenvalues of the Dirichlet eigenvalue problem

$$(\widehat{p}v')' + \widehat{\lambda}\widehat{\rho}v = 0, \quad \text{in } (0, 1)\,, \tag{76}$$

$$v(0) = 0 = v(1)\,, \tag{77}$$

with

$$\widehat{p} = \widehat{R}^{-1}, \quad \widehat{\rho} = \widehat{P}^{-1} \quad \text{in } [0, 1], \tag{78}$$

and vice versa, see [38]. Analogously, the positive eigenvalues of (74)–(75) are the Dirichlet eigenvalues of a damaged rod with axial stiffness $\widehat{p} = \widehat{R}^{-1}$ and mass density $\rho = P^{-1}$. Note that, by definition, the coefficients $\widehat{p}$, $\widehat{\rho}$, ρ are uniformly positive, smooth and even functions in $[0, 1]$.

The above mentioned equivalence between Neumann and Dirichlet eigenvalue problems allows us to adapt the procedure illustrated in Section 3 to the present case. Since most of the steps in the previous analysis

can be repeated, here we shall simply state the main new points and we omit the details of the proofs.

In brief, starting from the undamaged free-free rod with axial stiffness $\widehat{P}$ and mass density $\widehat{R}$, we introduce the equivalent undamaged supported rod with axial stiffness $\widehat{p} = \widehat{R}^{-1}$ and mass density $\widehat{\rho} = \widehat{P}^{-1}$. Next, we repeat the Steps 1-3 in Section 3 from the undamaged rod ($\widehat{p} = \widehat{R}^{-1}, \widehat{\rho} = \widehat{P}^{-1}$) to the reconstructed damaged rod ($p = \widehat{p} = \widehat{R}^{-1}, \rho = P^{-1}$). It should be noted that the roles of p and ρ are reversed with respect to the previous analysis, since the coefficient p takes the undamaged value, whereas the coefficient ρ varies. The reduction to impedance-type form and the construction of an impedance-type operator A with the first N Dirichlet eigenvalues presented in Sections 3.1 and 3.2, respectively, can be repeated step by step. The reversal Sturm–Liouville transformation (28)–(32) (with $\wp = p$) can be applied to the problem (23)–(24) to obtain the eigenvalue problem

$$\frac{d}{dz}\left(Qp(z)\frac{dv(z)}{dz}\right) + \lambda\frac{\widehat{M}^2}{Q}\rho(z)v(z) = 0, \quad z \in (0,1)\,, \tag{79}$$

$$v(0) = 0 = v(1)\,, \tag{80}$$

where we impose

$$Qp(z) = \widehat{p} = \widehat{R}^{-1}, \quad \text{in } [0,1], \tag{81}$$

and

$$\frac{\widehat{M}^2}{Q}\rho(z) = P^{-1}(z), \quad \text{in } [0,1], \tag{82}$$

with $\widehat{M}^2$ a known constant. To determine the unknown function $\frac{\rho(z)}{Q}$, we proceed as in Section 3.3 and we conclude that

$$\frac{\rho(z)}{Q} = \widehat{p}(z)(\overline{\eta}'(z))^2, \tag{83}$$

where $\overline{\eta} = \frac{\rho(z)}{Q}$, defined as in (44), is the unique solution to the Cauchy problem

$$\overline{\eta}'(z) = \frac{A(\overline{\eta}(z))}{\widehat{p}(z)}, \quad z \in \left(\frac{1}{2}, 1\right)\,, \tag{84}$$

$$\overline{\eta}\left(\frac{1}{2}\right) = \frac{1}{2}\,, \tag{85}$$

and $\overline{\eta}(1-z) = \overline{\eta}(z)$ in $[0,1]$. The solution to (84)–(85) can be determined numerically as it was explained, for example, in Section 4.3. Finally, by (82), $P^{-1}(z)$ is known and, using again the equivalence between the Dirichlet and Neumann problems, the reconstruction is completed.

7 Physical-based filtering

In previous sections we have provided a constructive algorithm for our inverse problem with finite eigendata. The most important mathematical tool used was the explicit determination of quasi-isospectral Sturm–Liouville operators of the type $(p, \widehat{\rho})$, with given/fixed $\widehat{\rho}$ and unknown p. One of the interesting, and partially surprising results, was the ability of the method to furnish good approximations of the unknown coefficient in L^∞-norm, which is generally possible only using an infinite number of data.

In this Section we show that, when the method is combined with additional information about the unknown stiffness coefficient, such as monotonicity or a priori information on the support of the stiffness variation, the approximation may further improve, leading to very good pointwise approximation of the solution. It is worth noticing that such additional information may frequently be available simply from the physics of the problem, see also [26]. More precisely, we shall consider in the sequel the following a priori information:

F$_1$) Structural damage can only reduce the initial stiffness $\widehat{p}$, that is

$$p(x) \le \widehat{p}(x), \quad \text{in } [0,1] \quad (\text{F}_1 \textit{ filtering}). \tag{86}$$

Actually, our mathematical procedure based on the explicit determination of quasi-isospectral Sturm-Liouville operators, produces stiffness profiles which oscillate near the undamaged stiffness $\widehat{p}$. Basing on this assumption $F1$, we may *filter* the outcome of the method by assuming vanishing increase of the axial stiffness.

F$_2$) As discussed in section 5.2.1, our method always produces significant stiffness reduction localized at the ends of the rod. If we a priori know, for example by means of other non destructive methods, that these regions actually are free of damage, then we can a priori set

$$p(x) = \widehat{p}(x), \quad \text{in } (0,\delta) \cup (1-\delta, 1) \quad (\text{F}_2 \textit{ filtering}) \tag{87}$$

for a given/assigned δ.

F$_3$) There are situations in which it is a priori known that a single localized damage occurs in the system, that is, the support of the stiffness variation $\widehat{p} - p$ is a (small) closed interval compactly contained in $[0, 1/2]$, *e.g.*,

$$\text{supp}(\widehat{p}(x) - p(x)) = [a,b]\,, \quad \text{with } 0 < a < b < 1/2 \quad (\text{F}_3 \textit{ filtering})\,. \tag{88}$$

In this case, under the assumption that the reconstructed stiffness is a good approximation of the actual damaged stiffness, it is enough to determine the interval of maximum stiffness reduction, and neglect all the possible remaining damaged regions. Application of this filter needs the specification of a cut-off value of the stiffness reduction, and may be not straightforward extendable to diffuse or multiple damages.

In order to check how the identification results improve by adding the above additional hypotheses, we tested the method in an extended series of simulations with error free data and Dirichlet end conditions. The following results are representative of the above filtering effects, and their possible combinations.

The first series of test concerns with the identification of a small single damage with $b = 0.24$, $c = 0.025$, $e = 0.2$ ($N = 20$). Figures 12(a)-(d) report the results obtained by applying separately filter F_1 and filter F_2 (with $\delta = 0.05$), and by combining in cascade $F_1 + F_2$ and $F_1 + F_2 + F_3$. By the analysis of these figures and by the comparison with the corresponding unfiltered results shown in Figure 5(b), it clearly emerges that filter F_2 has the strongest effect on the reconstruction results. Moreover, the accuracy of identification significantly improves in presence of cascade filter combinations.

The second test concerns the reconstruction of a single diffuse damage with intermediate severity (*e.g.*, $b = 0.24$, $c = 0.1$ and $e = 0.2$) using the first 20 frequencies. The results are presented in Figures 13 and are analogous to those depicted in Figure 12.

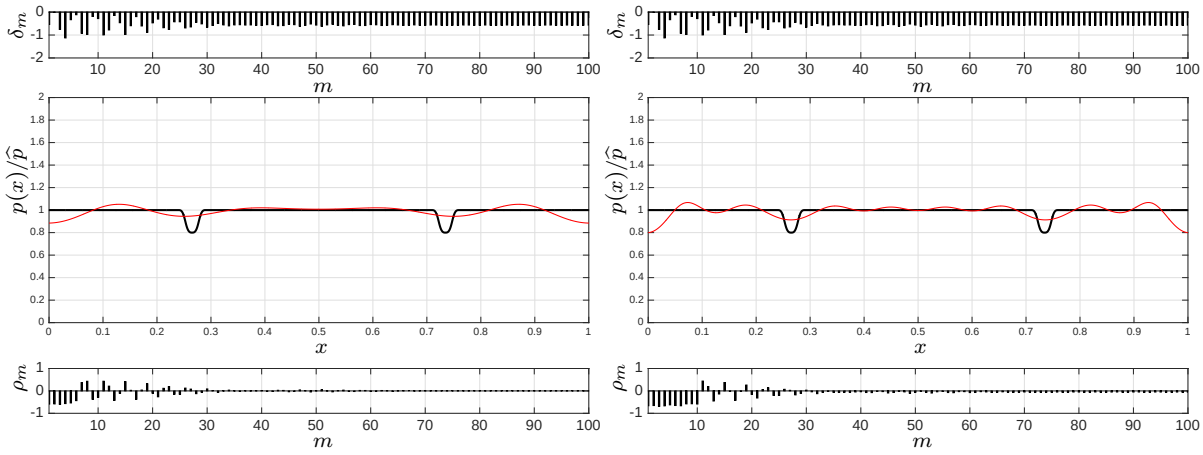

(a) $N = 5$ (b) $N = 10$

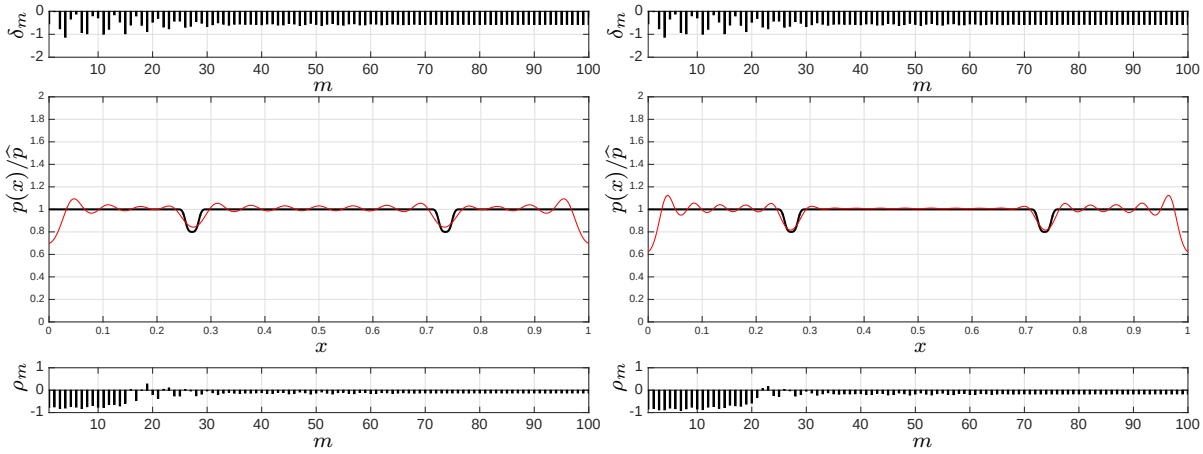

(c) $N = 15$ (d) $N = 20$

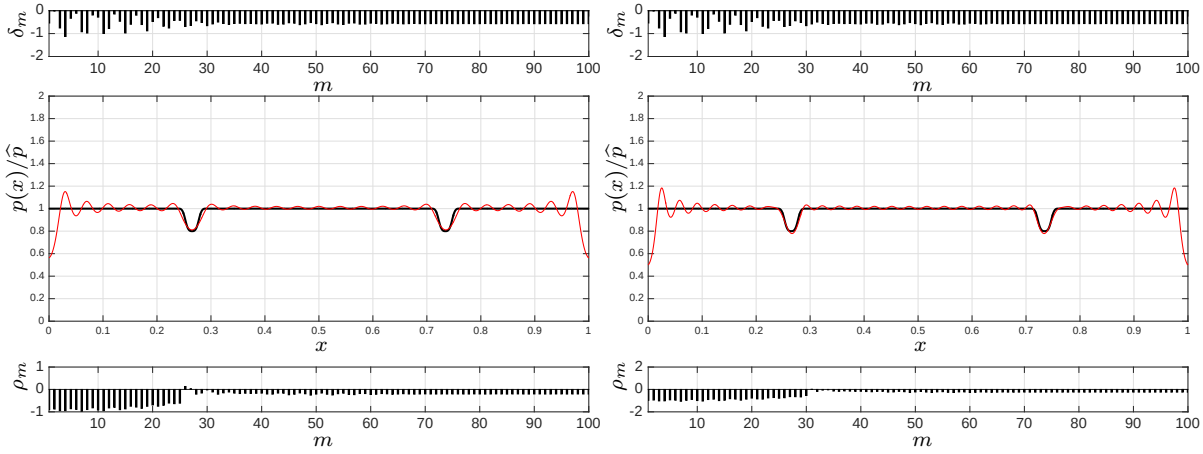

(e) $N = 25$ (f) $N = 30$

Fig. 3 Damage reconstruction varying the number of the first used frequencies N for $b = 0.24$, $c = 0.025$, $e = 0.2$.

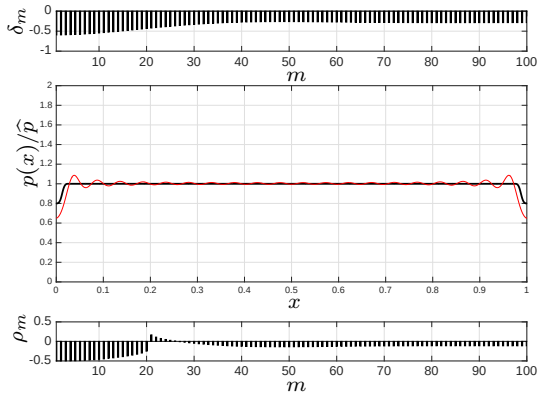

(a) $b = 0$

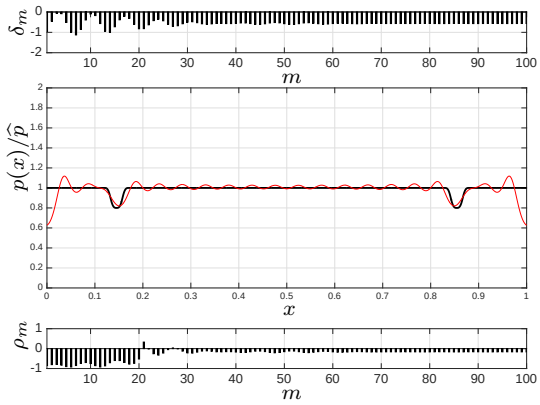

(b) $b = 0.12$

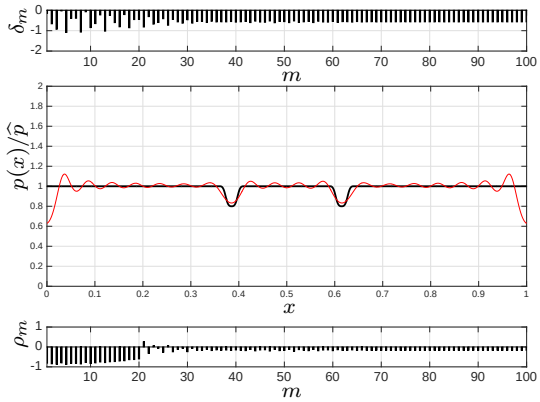

(c) $b = 0.36$

Fig. 4 Damage reconstruction varying the position b for $c = 0.025$, $e = 0.2$ and $N = 20$.

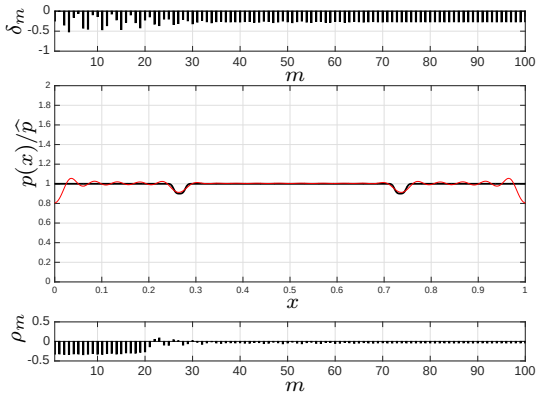

(a) $e = 0.1$

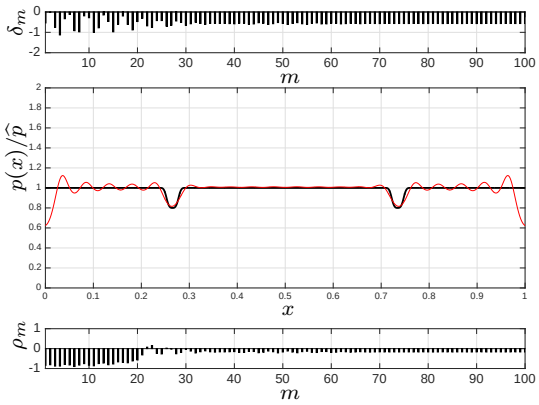

(b) $e = 0.2$

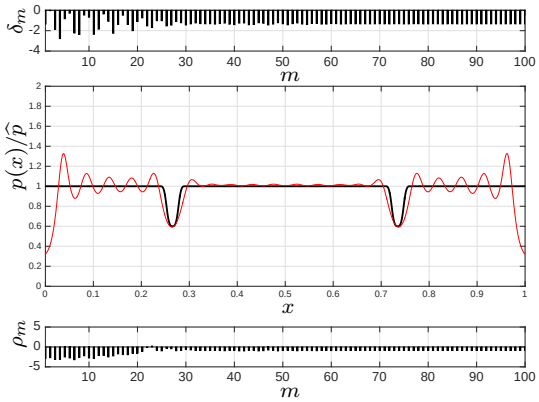

(c) $e = 0.4$

Fig. 5 Damage reconstruction varying the severity e for $b = 0.24$, $c = 0.025$ and $N = 20$.

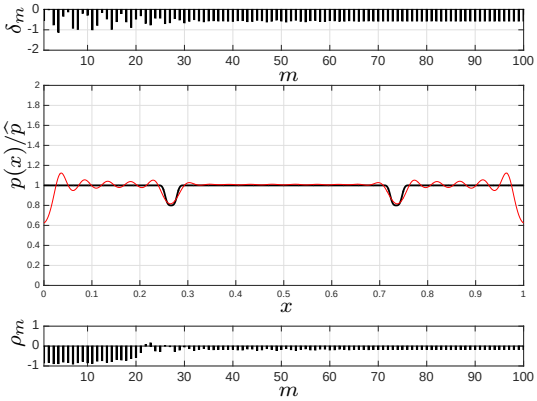

(a) $c = 0.025$

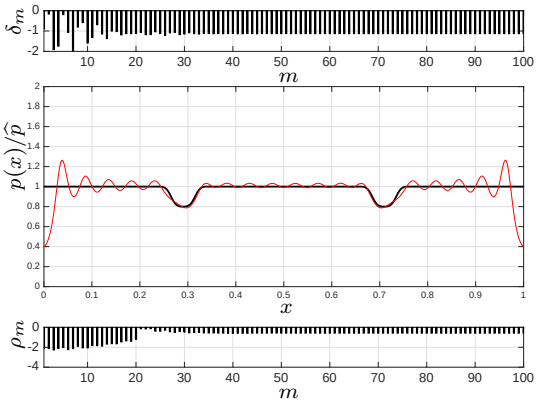

(b) $c = 0.050$

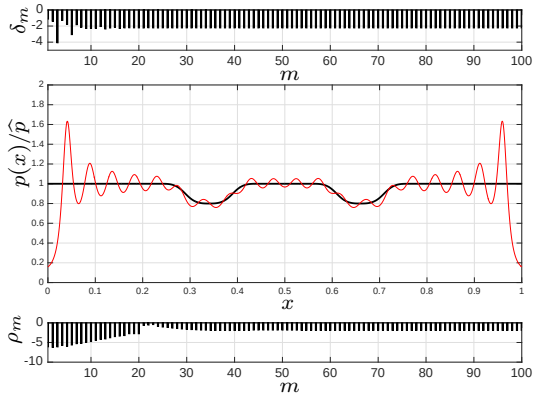

(c) $c = 0.100$

Fig. 6 Damage reconstruction varying the damage extension c for $b = 0.24$, $e = 0.2$ and $N = 20$.

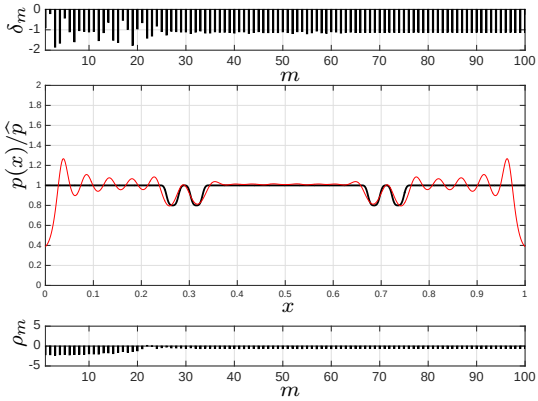

(a) $\beta = 0$

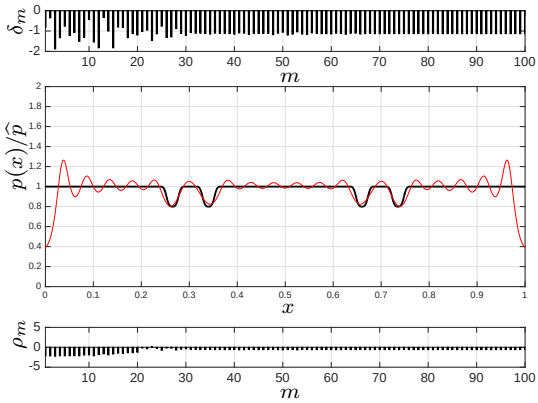

(b) $\beta = 1$

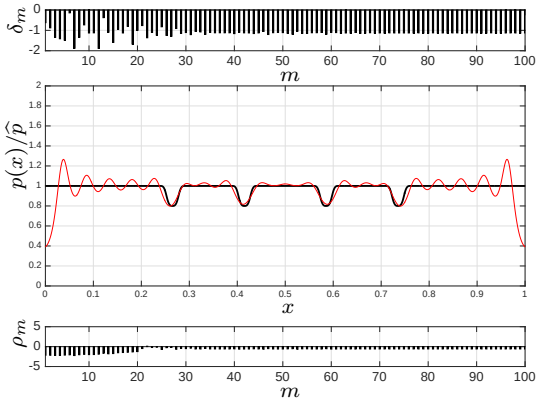

(c) $\beta = 4$

Fig. 7 Damage reconstruction of multiple localized damages for $b = 0.240$, $c = 0.025$, $e = 0.2$, $N = 20$, varying the distance βc between the damaged regions.

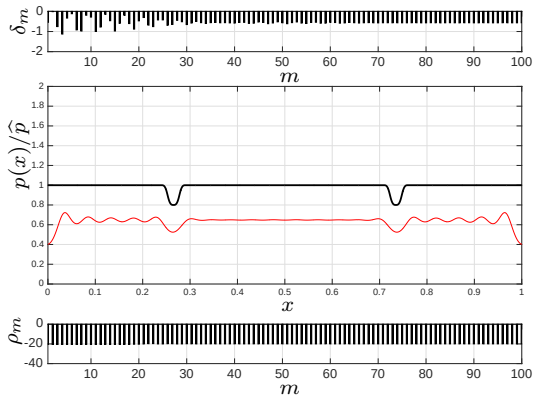

(a)

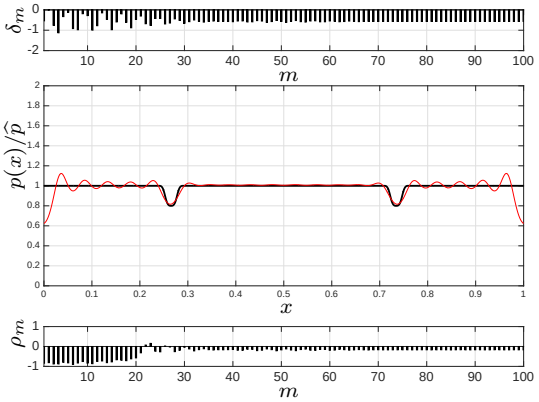

(b)

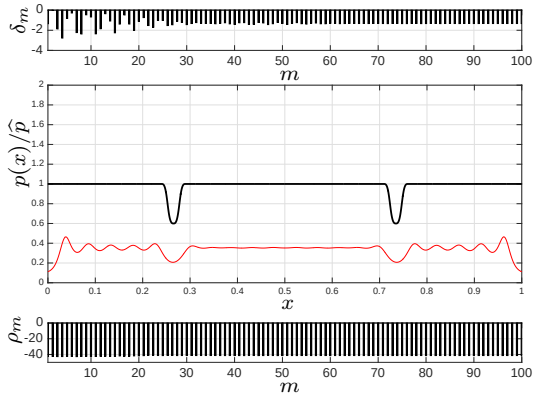

(c)

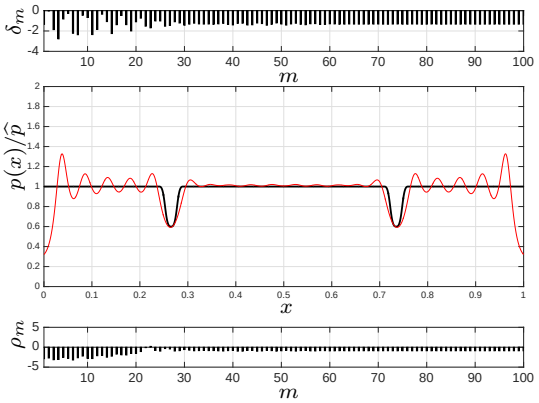

(d)

Fig. 8 Damage reconstruction with $N = 20$ without ((a) and (c)) and with ((b) and (d)) the additional information on $\int_0^1 p(x)dx$ for $b = 0.240$, $c = 0.025$, $e = 0.2$ ((a) and (b)) and $b = 0.240$, $c = 0.025$, $e = 0.4$ ((c) and (d)).

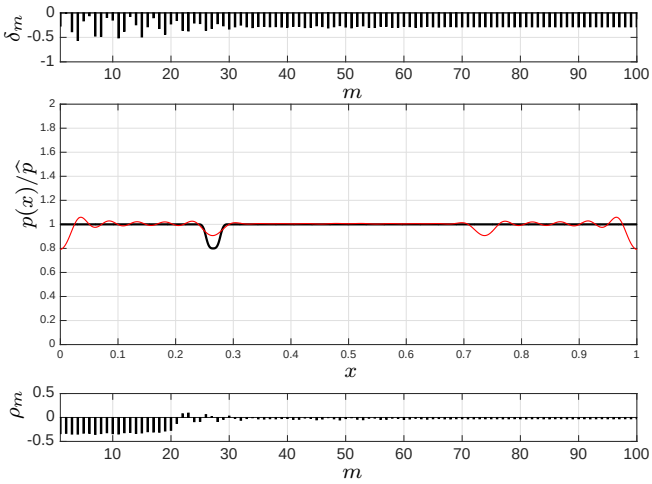

(a)

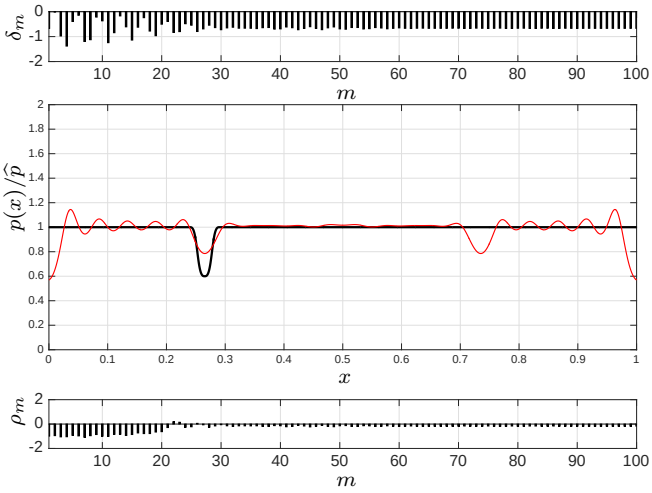

(b)

Fig. 9 Damage reconstruction of unsymmetrical damage for $b = 0.240$, $c = 0.025$, $e = 0.2$ (a) and $b = 0.240$, $c = 0.025$, $e = 0.4$ (b) and $N = 20$.

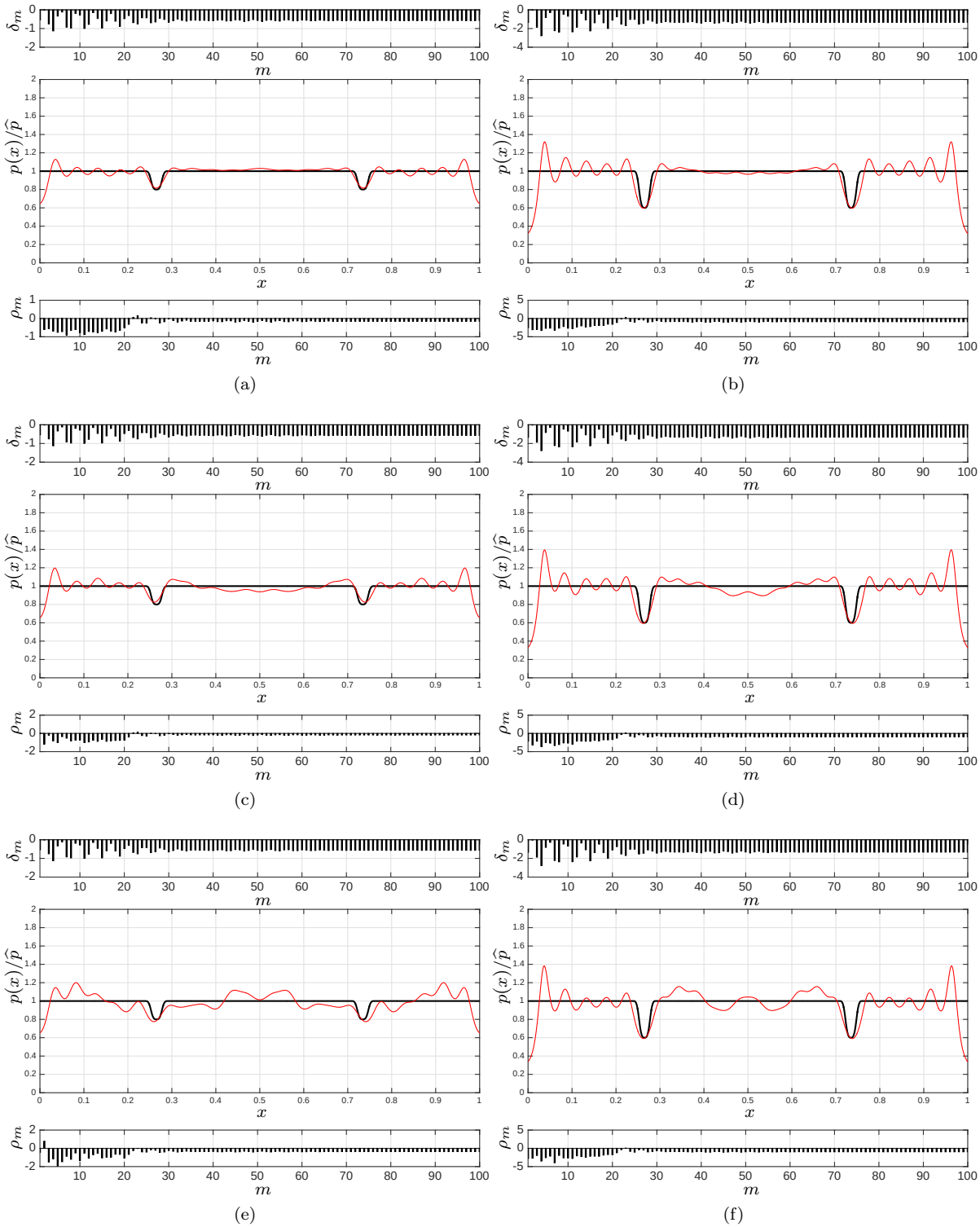

Fig. 10 Damage reconstruction with noise on the data as in Eq. (70) for $b = 0.24$, $c = 0.025$, $N = 20$. (a) $e = 0.2$, $\eta_{\max} = 0.01$; (b) $e = 0.4$, $\eta_{\max} = 0.01$; (c) $e = 0.2$, $\eta_{\max} = 0.03$; (d) $e = 0.4$, $\eta_{\max} = 0.03$; (e) $e = 0.2$, $\eta_{\max} = 0.05$; (f) $e = 0.4$, $\eta_{\max} = 0.05$. Black (thick) curve: target solution; red thin curve: reconstructed damage.

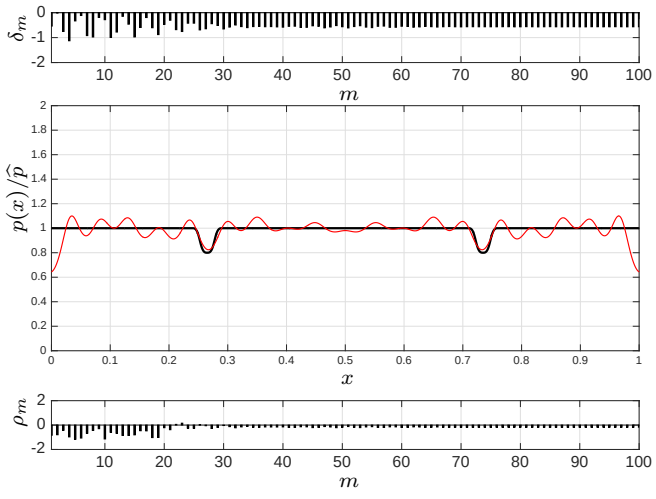

(a)

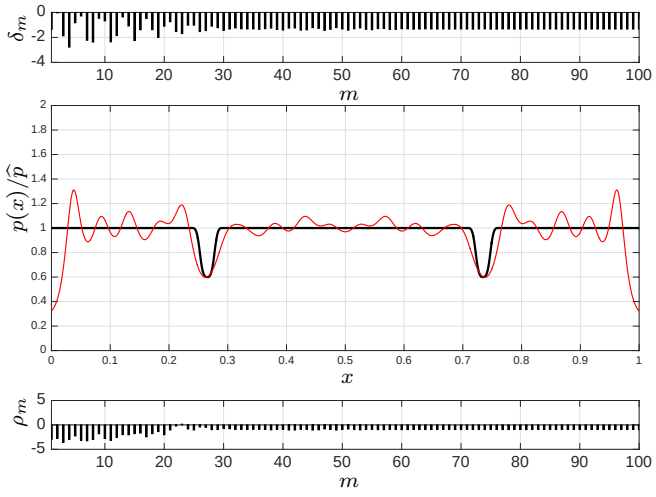

(b)

Fig. 11 Damage reconstruction with noise on the data as in Eq. (71) for $b = 0.24$, $c = 0.25$, $N = 20$, $\eta_{\max} = 0.005$. (a) $e = 0.2$; (b) $e = 0.4$. Black thick curve: target solution; red thin curve: reconstructed damage.

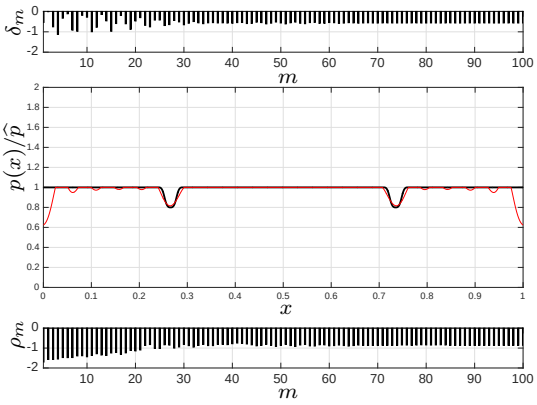

(a) F_1 filtering

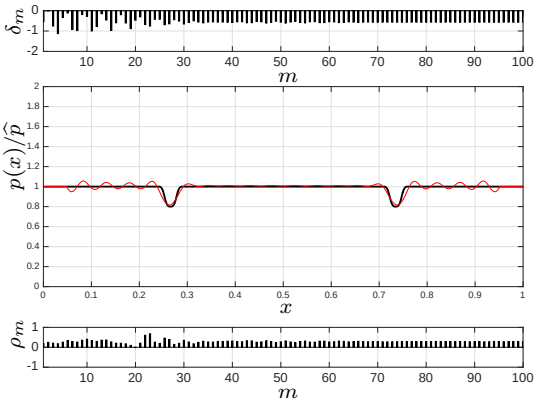

(b) F_2 filtering ($\delta = 0.05$)

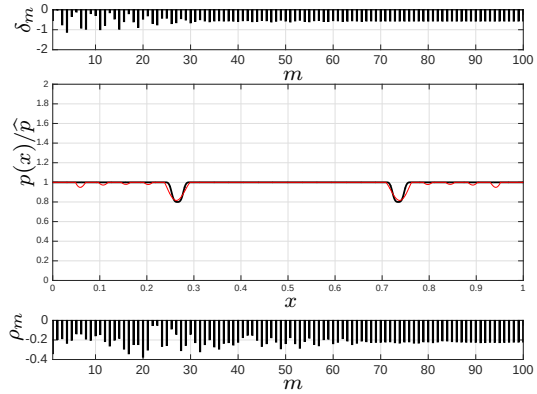

(c) $\mathrm{F}_1 + \mathrm{F}_2$ filtering

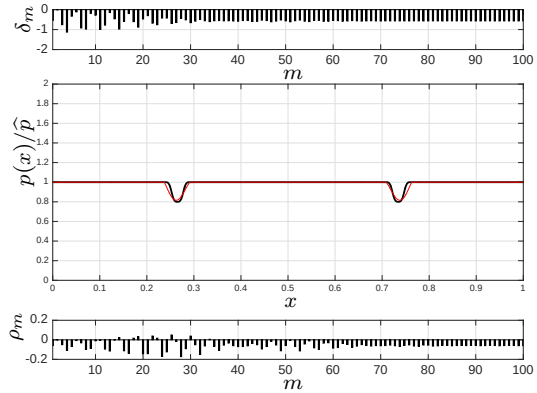

(d) $\mathrm{F}_1 + \mathrm{F}_2 + \mathrm{F}_3$ filtering

Fig. 12 Filtering effects on damage reconstruction for $b = 0.24$, $c = 0.025$, $e = 0.2$ and $N = 20$.

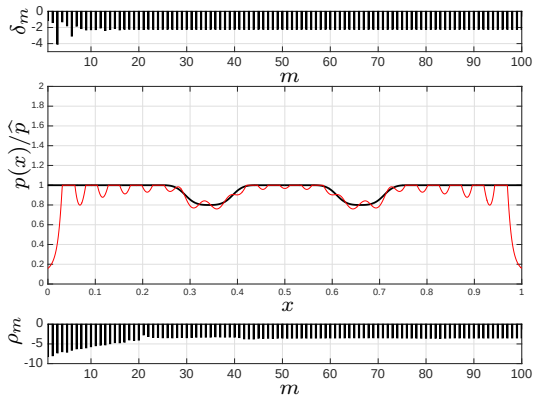

(a) F_1 filtering

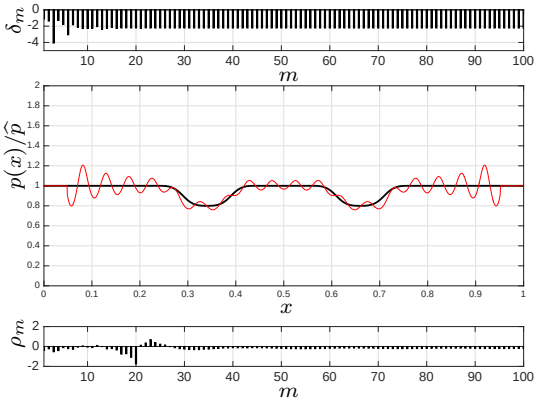

(b) F_2 filtering ($\delta = 0.05$)

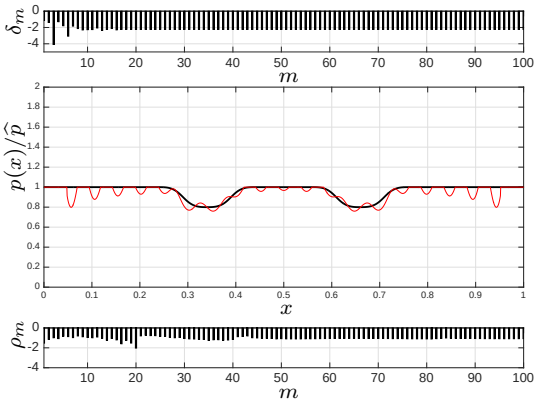

(c) F_1 + F_2 filtering

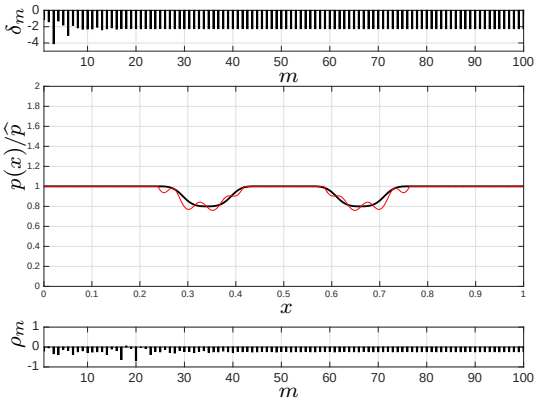

(d) F_1 + F_2 + F_3 filtering

Fig. 13 Filtering effects on damage reconstruction for $b = 0.24$, $c = 0.1$, $e = 0.2$ and $N = 20$.

8 An application to experimental data

The results of an experimental application of the diagnostic method are presented in this section. The specimen is the steel rod of square solid cross-section with side 0.022 m and length $L = 2.925$ m shown in Figure 14.

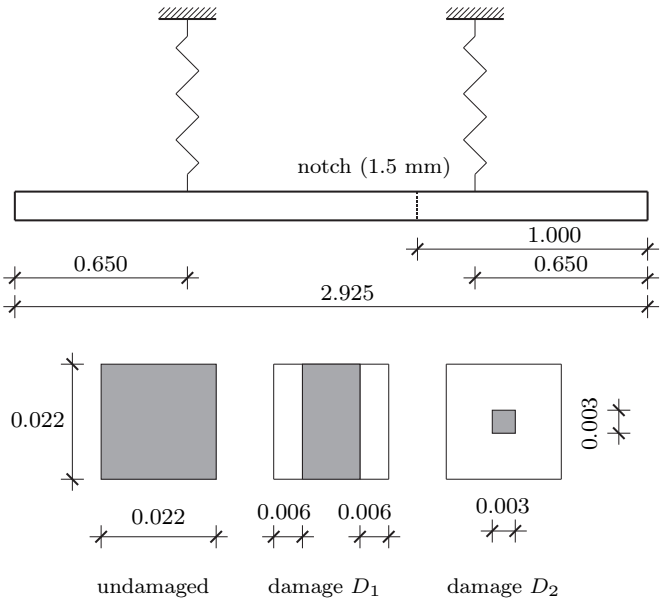

Fig. 14 Experimental model of axially vibrating rod and damage configurations (lengths in meters).

The rod was damaged by saw-cutting the transversal cross-section at the distance $s = 1.000$ m from one end, and two damage configurations D_1 and D_2 have been considered. An impulsive dynamic technique was used to measure the first 30 natural frequencies of the undamaged and damaged rod. Referring to [29] for more details on the experiments, we recall that the rod was suspended by two soft steel wire ropes to simulate Neumann end conditions (73). Natural frequencies were estimated from the frequency response function obtained by exciting one end by means of an impulse force hammer and acquiring the axial response by a piezoelectric accelerometer at the other end of the rod. Signals were processed by using a dynamic analyzer HP35650. Table 3 collects the natural frequency values. The analytical model of the undamaged rod was determined by assuming axial stiffness and mass density per unit length equal to 9.9491×10^7 N and 3.735 kg/m, respectively. The model turns out to be extremely accurate, with percentage errors lower than 0.2% within the first 20 vibrating modes. Eigenfrequency shifts caused by the damage are, in average, of order $0.3 - 0.4\%$ and $1 - 4\%$ of the initial frequency values for damage D_1 and D_2, respectively. It can be seen that there are few vibration modes with small increasing of natural frequency. As it was observed in [29], the origin of this unexpected behaviour is probably due to measurement errors made in estimating the resonant frequencies from the frequency response functions.

Before presenting the results, it should be noticed that the study of this experimental problem is a severe and challenging test of the proposed identification method. In fact, the damage corresponds to rather abrupt change of the axial stiffness coefficient concentrated on a small interval of the rod axis. Moreover, the lack of symmetry of the damaged configuration with respect to the mid-point of the rod axis may introduce further indeterminacy, as it was discussed in Section 5.2.4.

The results of identification are summarized in Figures 15 and 16 for increasing number N of frequency data. The scaling factor was determined by prescribing the undamaged value of the axial stiffness at the midpoint of the rod axis. The identified axial stiffness shows a reduction exactly near the actual damage location (and its symmetric position), even if, as it is expected, modelling errors partially mask the changes induced by damage in configuration $D1$. The results show a good stability of the identification with respect to N, and the first $15 - 20$ natural frequencies are sufficient for a fairly accurate reconstruction of the damage. As for Dirichlet end conditions, the identified stiffness coefficient shows a wavy behavior around the undamaged value. The amplitude of the oscillations reduces as N increases, with the exception of small neighborhoods of the ends of the rod. In particular, it can be proved that the value of the identified stiffness taken at the end of the rod increases as N increases and, therefore, it can be significantly higher than the undamaged value. Finally, the application of the physical-based filters introduced in Section 7 produces an important improvement of the quality of identification. As an example, Figure 17 shows the results obtained using the filter $F_1 + F_2 + F_3$ with $N = 20$.

9 Conclusions

This paper was devoted to the study of a basic, fundamental diagnostic problem in structural dynamics, namely the identification of damage in an axially vibrating rod from the knowledge of the first N natural frequencies under supported end conditions. It was assumed that the damage does not affect the mass density and that it reflects into a reduction of the axial stiffness of the rod only. Moreover, in order to have uniqueness of the solution (at least as $N \to \infty$), both the undam-

Table 3 Experimental frequencies of the rod of Fig. 14 and analytical values for the undamaged configuration (the rigid body motion is omitted). Undamaged configuration: $\Delta_n\% = 100 \cdot (f_n^{\rm model} - f_n^{\rm exp})/f_n^{\rm exp}$. Damage scenarios $D1$ and $D2$: $\Delta_n\% = 100 \cdot (f_n^{\rm dam} - f_n^{\rm undam})/f_n^{\rm undam}$. Frequency values in Hz.

Mode	Undamaged			Damage D_1		Damage D_2	
n	Exper.	Model	$\Delta_n\%$	Exper.	$\Delta_n\%$	Exper.	$\Delta_n\%$
1	882.25	882.25	-0.00	879.30	-0.33	831.00	-5.81
2	1764.60	1764.50	-0.01	1759.00	-0.32	1679.50	-4.82
3	2645.80	2646.74	0.04	2647.00	0.05	2646.50	0.03
4	3530.30	3528.99	-0.04	3516.50	-0.39	3306.00	-6.35
5	4411.90	4411.24	-0.01	4400.00	-0.27	4250.00	-3.67
6	5293.90	5293.49	-0.01	5295.30	0.03	5287.80	-0.12
7	6175.40	6175.74	0.01	6150.30	-0.41	5808.50	-5.94
8	7056.70	7057.98	0.02	7039.50	-0.24	6864.30	-2.73
9	7937.90	7940.23	0.03	7938.00	0.00	7909.50	-0.36
10	8819.90	8822.48	0.03	8782.00	-0.43	8340.00	-5.44
11	9702.70	9704.73	0.02	9682.80	-0.21	9503.30	-2.06
12	10583.80	10586.98	0.03	10581.30	-0.02	10514.80	-0.65
13	11464.30	11469.23	0.04	11410.50	-0.47	10933.50	-4.63
14	12345.20	12351.47	0.05	12331.50	-0.11	12158.00	-1.52
15	13224.40	13233.72	0.07	13322.00	0.74	13098.00	-0.96
16	14104.00	14115.97	0.08	14039.00	-0.46	13543.00	-3.98
17	14985.00	14998.22	0.09	14964.00	-0.14	14811.00	-1.16
18	15862.00	15880.47	0.12	15850.00	-0.08	15676.00	-1.17
19	16740.00	16762.71	0.14	16662.00	-0.47	16177.00	-3.36
20	17620.00	17644.96	0.14	17596.00	-0.14	17464.00	-0.89
21	18496.00	18527.21	0.17	18478.00	-0.10	18237.00	-1.40
22	19372.00	19409.46	0.19	19283.00	-0.46	18820.00	-2.85
23	20248.00	20291.71	0.22	20227.00	-0.10	20111.00	-0.68
24	21124.00	21173.95	0.24	21102.00	-0.10	20801.00	-1.53
25	21999.00	22056.20	0.26	21906.00	-0.42	21441.00	-2.54
26	22870.00	22938.45	0.30	22872.00	0.01	22815.00	-0.24
27	23744.00	23820.70	0.32	23724.00	-0.08	23357.00	-1.63
28	24621.00	24702.95	0.33	24532.00	-0.36	24137.00	-1.97
29	25495.00	25585.19	0.35	25512.00	0.07	25514.00	0.07
30	26372.00	26467.44	0.36	26344.00	-0.11	25919.00	-1.72

aged and damaged rod were assumed to be symmetric with respect to the mid-point of the rod axis.

The inverse problem was solved by means of repeated determinations of quasi-isospectral rod operators having the same mass density of the undamaged rod and with axial stiffness such that all resonant frequencies coincide with those of the initial undamaged rod, with the exception of a single frequency which is taken coincident with the target value of the damaged rod. The method was implemented numerically and tested on rods with various damage scenarios, including single and multiple damages of different shape, position and intensity.

The results of an extensive series of simulations show that identification of damage is effective when the first fifteen-twenty natural frequencies are employed, and when the damaged rod is a small perturbation of the initial undamaged rod. For these cases, which are of importance as early alarms in practical applications, the method was able to identify both the number and the shape of the axial stiffness changes with high degree of accuracy, even in presence of multiple localized damages. Simulations performed on noisy frequency data show that reconstruction procedure is sufficiently stable, provided that the errors are smaller than the damage induced changes in the natural frequencies used in identification. An intrinsic feature of the method is the wavy behavior of the reconstructed axial stiffness occurring near the ends of the rod, which, in case of severe damages located close to these regions, may obstruct the correct identification of the system. In the last part of the paper it has been shown how to include a priori information coming from the physics of the problem in order to reduce this indeterminacy and improve the results of the reconstruction. An extension of the method to rods under free-free end conditions was also presented and tested for the identification of localized damage from experimental frequency data.

As a final remark, we point out that a theoretical aspect worth of investigation that emerges from our analysis stands on the possibility of determining stability estimates of the axial stiffness of the damaged

system in terms of the first N natural frequencies used in identification. It is likely that the results and methods presented in [25], [20] and [28] may be useful for this purpose.

A

In this Appendix we show how to construct an impedance coefficient $A^*(x)$ such that all the Dirichlet eigenvalues of $A^*(x)$ coincide with those of the (given) coefficient $\widehat{A}(x)$, with the exception of the nth eigenvalue, where n is a given integer, $n \geq 1$. The impedance operators associated to $\widehat{A}(x)$ and $A^*(x)$ are said *quasi-isospectral*. It should be noticed that, once a constructive method for the determination of a quasi-isospectral operator is available, then a repeated application of the procedure leads to the coefficient $A(x)$ in (23)–(24).

By applying the classical Liouville transformation

$$\widehat{A}(x) = \widehat{a}^2(x), \quad y(x) = \widehat{a}(x)u(x), \tag{89}$$

where $\widehat{a} = \widehat{a}(x)$ can be chosen of one-sign in $[0,1]$ (positive, say), the eigenvalue problem (16)–(17) can be written in Sturm-Liouville canonical form as follows

$$y''(x) + \mu y(x) = \widehat{q}(x)y(x), \qquad x \in (0,1), \tag{90}$$
$$y(0) = 0 = y(1). \tag{91}$$

The Schröedinger potential

$$\widehat{q}(x) = \frac{\widehat{a}''(x)}{\widehat{a}(x)}\,, \tag{92}$$

is a continuous function in $[0,1]$. The eigenfunctions associated to the eigenvalues $\widehat{\mu}_m = \mu_m(\widehat{q})$ (or $\widehat{\mu}_m = \mu_m(\widehat{A})$) of (90)–(91) are denoted by $\{z_m(x)\}_{m=1}^{\infty}$, and are normalized so that

$$z'_m(0) = 1, \qquad m = 1, 2, \cdots. \tag{93}$$

Let n, $n \geq 1$, be a given integer and let the shift parameter $t \in \mathbb{R}$ be such that

$$\widehat{\mu}_{n-1} < \widehat{\mu}_n + t < \widehat{\mu}_{n+1}, \tag{94}$$

with $\widehat{\mu}_0 = 0$. It should be noticed that, in our diagnostic problem, $\widehat{\mu}_n + t$ coincides with the nth eigenvalue of the damaged rod μ_n. Therefore, inequalities (94) are always satisfied taking $-(\widehat{\mu}_n - \widehat{\mu}_{n-1}) < t < 0$. Let us introduce the *fundamental solutions* $y_1 = y_1(x, \widehat{q}, \widehat{\mu}_n + t)$, $y_2 = y_2(x, \widehat{q}, \widehat{\mu}_n + t)$ to the following Cauchy's problems

$$y_1'' + (\widehat{\mu}_n + t)y_1 = \widehat{q}y_1, \qquad x \in (0,1), \tag{95}$$
$$y_1(0) = 1, \tag{96}$$
$$y_1'(0) = 0, \tag{97}$$

and

$$y_2'' + (\widehat{\mu}_n + t)y_2 = \widehat{q}y_2, \qquad x \in (0,1), \tag{98}$$
$$y_2(0) = 0, \tag{99}$$
$$y_2'(0) = 1. \tag{100}$$

A direct calculation shows that the function

$$w_{n,t}(x, \widehat{q}, \widehat{\mu}_n + t) = y_1(x, \widehat{q}, \widehat{\mu}_n + t) + \frac{y_1(1, \widehat{\mu}_n) - y_1(1, \widehat{\mu}_n + t)}{y_2(1, \widehat{\mu}_n + t)} y_2(x, \widehat{q}, \widehat{\mu}_n + t)\,, \tag{101}$$

is the solution to

$$w''_{n,t} + (\widehat{\mu}_n + t)w_{n,t} = \widehat{q}w_{n,t}, \qquad x \in (0,1), \tag{102}$$
$$w_{n,t}(0) = 1, \tag{103}$$
$$w_{n,t}(1) = y_1(1, \widehat{q}, \widehat{\mu}_n), \tag{104}$$

for $t \neq 0$. The function $w_{n,t}$ is well-defined for all $t \neq 0$ and has a removable singularity at $t = 0$. Finally, let us define

$$\omega_{n,t}(x, \widehat{q}, \widehat{\mu}_n + t) = [w_{n,t}, z_n], \tag{105}$$

where $[f, g] = fg' - f'g$, for every regular functions f and g. The function $\omega_{n,t}$ is a continuous and strictly positive function in $[0,1]$ for every $\widehat{q} \in C([0,1])$ and for every t satisfying (94), $n \geq 1$. Moreover, $\omega_{n,t}$ turns out to be a C^2-function of the variable x in $[0,1]$, see [35].

Under the above notation, it can be shown that for a given $n \geq 1$ the impedance coefficient

$$A^*(x) = (a^*(x))^2, \tag{106}$$

where

$$a^* = \widehat{a} - t\frac{w_{n,t}}{\widehat{\mu}_n \omega_{n,t}}[z_n, \widehat{a}], \quad \widehat{\mu}_{n-1} < \widehat{\mu}_n + t < \widehat{\mu}_{n+1}, \tag{107}$$

has exactly the same Dirichlet eigenvalues of the impedance coefficient $\widehat{A}(x) = \widehat{a}^2(x)$, with the exception of the nth eigenvalue, that is $\widehat{\mu}_m(\widehat{A}) = \mu_m(A^*)$ for every $m \geq 1$ with $m \neq n$, and $\mu_n(A^*) = \mu_n(\widehat{A}) + t$. The function $A^* = A^*(x)$ is the wished impedance coefficient quasi-isospectral to the initial impedance $\widehat{A} = \widehat{A}(x)$, see [31] for more details.

The function $a^* = a^*(x)$ defined in (107) corresponds to a "physical" impedance, since it can be proved that the function a^* is C^2-smooth and uniformly positive function in $[0,1]$ for every value of t satisfying the inequalities in (107). Moreover, if the initial coefficient $\widehat{A}(x)$ is an even function with respect to $x = \frac{1}{2}$, then, also the corresponding quasi-isospectral impedance $A^*(x)$ given by (106) is an even function with respect to $x = \frac{1}{2}$.

Acknowledgements The second author gratefully acknowledges the financial support of the National Research Project PRIN 2015TTJN95 "Identication and monitoring of complex structural systems".

The authors declare that they have no conflict of interest.

References

1. Adams, R.D., Cawley, P., Pye, C.J., Stone, B.J.: A vibration technique for non-destructively assessing the integrity of structures. Journal of Mechanical Engineering Science **20**(2), 93–100 (1978)
2. Aristodemo, M.: A high-continuity finite element model for two-dimensional elastic problems. Computers & Structures **21**(5), 987–993 (1985)
3. Aristodemo, M., Turco, E.: Boundary element discretization of plane elasticity and plate bending problems. International Journal for Numerical Methods in Engineering **37**, 965–987 (1994)
4. Barnes, D.C.: The inverse eigenvalue problem with finite data. SIAM Journal on Mathematical Analysis **22**(3), 732–753 (1991)

5. Bilotta, A., Formica, G., Turco, E.: Performance of a high-continuity finite element in three-dimensional elasticity. International Journal for Numerical Methods in Biomedical Engineering **26**, 1155–1175 (2010)
6. Bilotta, A., Morassi, A., Turco, E.: Reconstructing blockages in a symmetric duct via quasi-isospectral horn operators. Journal of Sound and Vibration **366**, 149–172 (2016)
7. Caddemi, S., Caliò, I.: Exact reconstruction of multiple concentrated damages on beams. Acta Mechanica **225**, 3137–3156 (2014)
8. Cazzani, A., Malagù, M., Turco, E.: Isogeometric analysis of plane curved beams. Mathematics and Mechanics of Solids **21**(5), 562–577 (2016)
9. Cerri, M.N., Vestroni, F.: Detection of damage in beams subjected to diffuse cracking. Journal of Sound and Vibration **234**(2), 259–276 (2000)
10. Courant, R., Hilbert, D.: Methods of Mathematical Physics, (first english edition) edn. Interscience Publishers Inc., New York (1966)
11. Darboux, G.: Sur la répresentation sphérique des surfaces. C. R. Acad. Sci. Paris **94**, 1343–1345 (1882)
12. Deuflhard, P.: Recent progress in extrapolation methods for ordinary differential equations. SIAM Review **27**(4), 505–535 (1985)
13. Dilena, M., Morassi, A.: Reconstruction method for damage detection in beams based on natural frequency and antiresonant frequency measurements. Journal of Engineering Mechanics **136**(3), 329–344 (2010)
14. Friswell, M.I., Mottershead, J.E.: Finite element model updating in structural dynamics. Kluwer Academic Publishers, Dordrecht, The Netherlands (1995)
15. Gladwell, G.M.L.: Inverse problems in vibration, 2nd edn. Kluwer Academic Publishers, Dordrecht, The Netherlands (2004)
16. Gladwell, G.M.L., England, A.H., Wang, D.: Examples of reconstruction of an Euler–Bernoulli beam from spectral data. Journal of Sound and Vibration **119**, 81–94 (1987)
17. Golub, G.H., Loan, C.F.V.: Matrix computations, 3rd edn. The Johns Hopkins University Press, Baltimore and London (1996)
18. Gragg, W.B.: On extrapolation algorithms for ordinary initial value problems. SIAM Journal on Numerical Analysis **2**, 384–404 (1965)
19. Hald, O.H.: Inverse eigenvalue problems for layered media. Communications on Pure and Applied Mathematics **XXX**, 69–84 (1977)
20. Hald, O.H.: The inverse Sturm–Liouville problem with symmetric potentials. Acta Mathematica **141**, 263–291 (1978)
21. Hearn, G., Testa, R.B.: Modal analysis for damage detection in structures. Journal of Structural Engineering **117**(10), 3042–3063 (1991)
22. Henrici, P.: Discrete Variable Methods in Ordinary Differential Equations. John Wiley, New York (1962)
23. Hochstadt, H.: The inverse Sturm–Liouville problem. Communications on Pure and Applied Mathematics **XXVI**, 715–729 (1973)
24. Hochstadt, H.: On inverse problems associated with Sturm–Liouville operators. Journal of Differential Equations **17**, 220–235 (1975)
25. Hochstadt, H.: On the well-posedness of the inverse Sturm–Liouville problems. Journal of Differential Equations **23**, 402–413 (1977)
26. Jiménez, R.D., Santos, L.C., Kuhl, N.M., J. C. Egaña, Soto, R.L.: An inverse eigenvalue procedure for damage detection in rods. Computers and Mathematics with Applications **47**, 643–657 (2004)
27. Lowe, B.D.: On the construction of an Euler–Bernoulli beam from spectral data. Journal of Sound and Vibration **163**(1), 165–171 (1993)
28. McLaughlin, J.: Stability theorems for two inverse spectral problems. Inverse Problems **4**, 529–540 (1988)
29. Morassi, A.: A uniqueness result on crack location in vibrating rods. Inverse Problems in Engineering **4**, 231–254 (1997)
30. Morassi, A.: Damage detection and generalized Fourier coefficients. Journal of Sound and Vibration **302**, 229–259 (2007)
31. Morassi, A.: Constructing rods with given natural frequencies. Mechanical Systems and Signal Processing **40**, 288–300 (2013)
32. Morassi, A., Vestroni, F. (eds.): Dynamic Methods for Damage Detection in Structures, *CISM Courses and Lectures*, vol. 499. Springer (2008)
33. Pau, A., Greco, A., Vestroni, F.: Numerical and experimental detection of concentrated damage in a parabolic arch by measured frequency variations. Journal of Vibration and Control **17**(4), 605–614 (2011)
34. Piegl, L., Tiller, W.: The NURBS Book, 2nd edn. Springer-Verlag Berlin Heidelberg (1997)
35. Pöschel, J., Trubowitz, E.: Inverse Spectral Theory. Academic Press (1987)
36. Röhrl, N.: A least-squares functional for solving inverse Sturm–Liouville problems. Inverse Problems **21**, 2009–2017 (2005)
37. Rubio, L.: An efficient method for crack identification in simply supported Euler–Bernoulli beams. Journal of Vibration and Acoustics **131**, 051,001 (2009)
38. Rubio, L., Fernández-Sáez, J., Morassi., A.: Crack identification in non-uniform rods by two frequency data. International Journal of Solids and Structures **75-76**, 61–80 (2015)
39. Sinha, J.K., Friswell, M.I., Edwards, S.: Simplified models for the location of cracks in beam structures using measured vibration data. Journal of Sound and Vibration **251**(1), 13–38 (2002)
40. Teughels, A., Maeck, J., De Roeck, G.: Damage assessment by FE model updating using damage functions. Computers and Structures **80**, 1869–1879 (2002)
41. Turco, E., Aristodemo, M.: A three-dimensional B-spline boundary element. Computer Methods in Applied Mechanics and Engineering **155**, 119–128 (1998)
42. Vestroni, F., Capecchi, D.: Damage detection in beam structures based on frequency measurements. Journal of Engineering Mechanics **126**, 761–768 (2000)

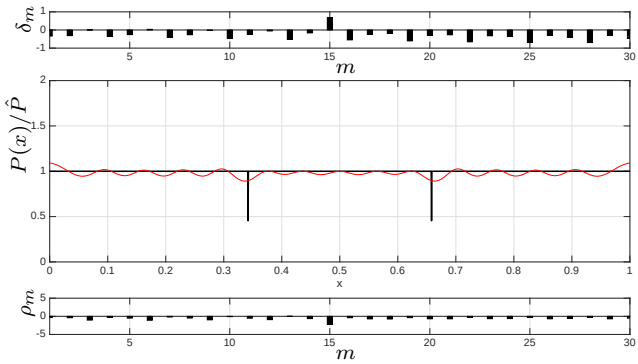

(a) $N = 15$

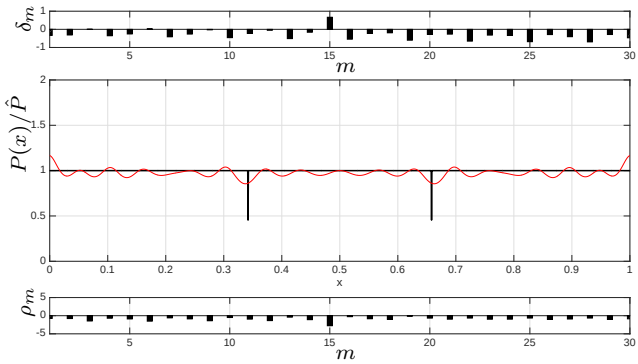

(b) $N = 20$

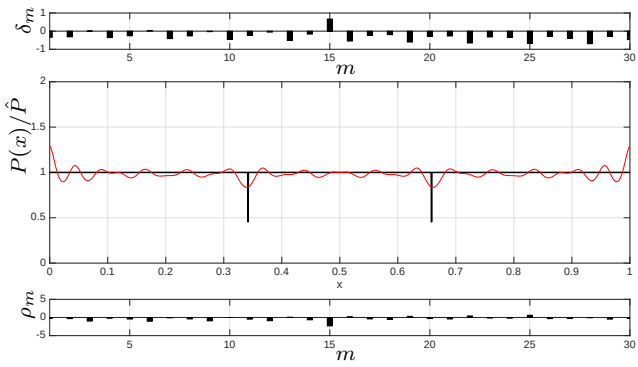

(c) $N = 25$

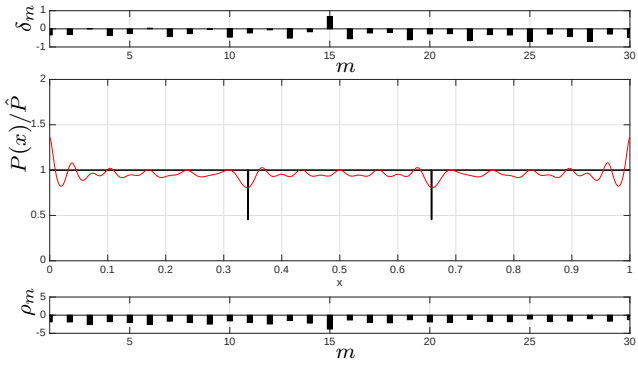

(d) $N = 30$

Fig. 15 Experimental model of Figure 14: identification of damage D_1 varying the number of the first natural frequencies N (the normalized abscissa is denoted by x, $x \in [0, 1]$).

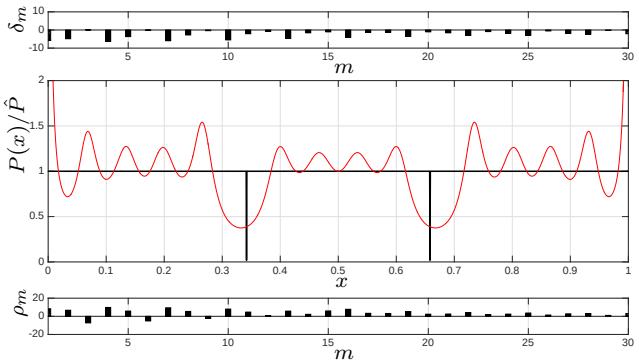

(a) $N = 15$

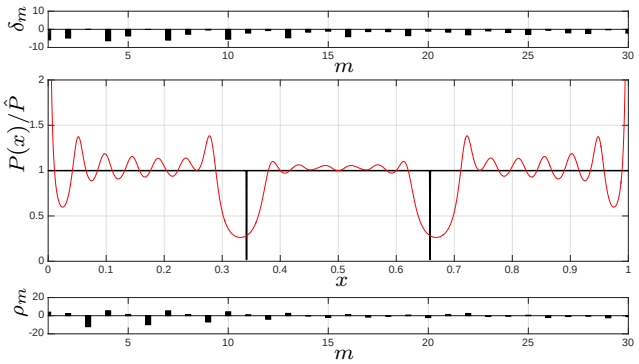

(b) $N = 20$

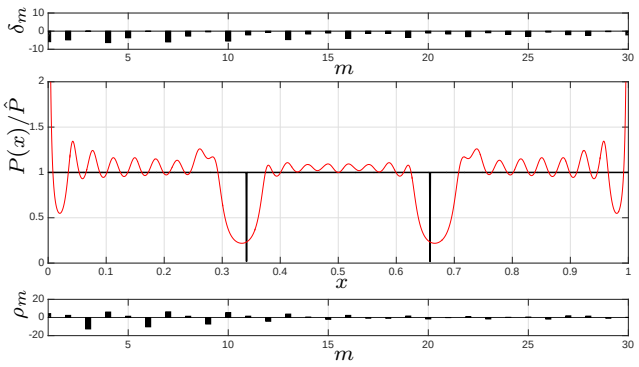

(c) $N = 25$

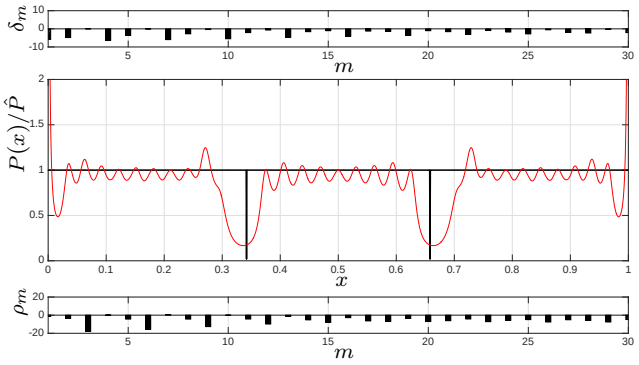

(d) $N = 30$

Fig. 16 Experimental model of Figure 14: identification of damage D_2 varying the number of the first natural frequencies N (the normalized abscissa is denoted by x, $x \in [0, 1]$).

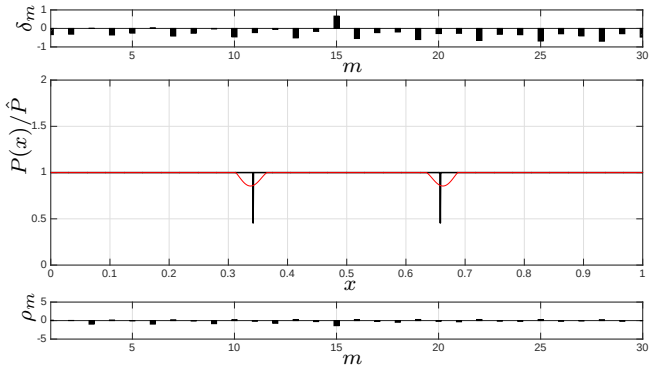

(a) Damage D_1

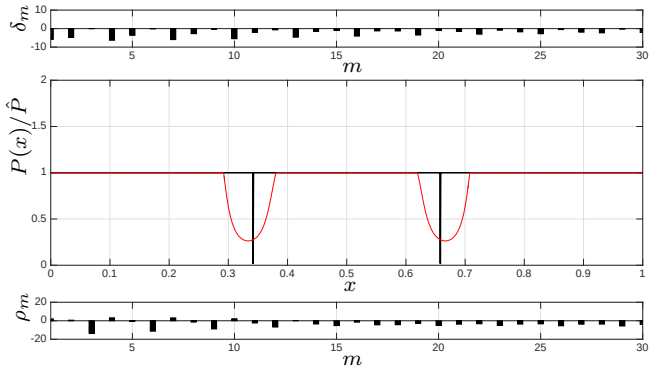

(b) Damage D_2

Fig. 17 Damage identification results for the rod of Figure 14 using the first 20 frequencies and the filter $F_1 + F_2 + F_3$ (the normalized abscissa is denoted by x, $x \in [0, 1]$).